TEMPERATURE DEPENDENT CONDUCTIVITY OF $NH_4^+/NiSO_4.7H_2O$ CRYSTAL

PhD DISSERTATION

EI EI MYO

DEPARTMENT OF PHYSICS

UNIVERSITY OF YANGON

MYANMAR

MAY 2011

TEMPERATURE DEPENDENT CONDUCTIVITY OF $NH_4^+/NiSO_4.7H_2O$ CRYSTAL

EI EI MYO

THIS DISSERTATION IS SUBMITTED TO THE BOARD OF EXAMINERS IN PHYSICS, UNIVERSITY OF YANGON FOR THE DEGREE OF DOCTOR OF PHILOSOPHY

EXTERNAL EXAMINER

CHAIRPERSON
Dr Win Win Thar
Professor and Head
Department of Physics
University of Yangon

REFEREE

MEMBER
Dr Nwe Ni Khin
Professor
Department of Physics
University of Yangon

MEMBER

SUPERVISOR
Dr Win Win Thar
Professor and Head
Department of Physics
University of Yangon

CO-SUPERVISOR
Dr Win Kyaw
Lecturer
Department of Physics
University of Yangon

CONTENTS

ACKNOWLEDGEMENTS

I would like to thank my Supervisor Professor Dr Win Win Thar, PhD(*UY*), Head of Department of Physics, University of Yangon, for her kind permission to carry out this work.

I am also grateful to my Co-supervisor Dr Win Kyaw, PhD(*UY*) MInstP(*London*), Lecturer in Physics, University of Yangon, for his valuable guidance.

I also wish to express my thanks to Professor Dr Pho Kaung, DSc(*Hokkaido*), MInstP(*London*), Pro-Rector and Director of ARC, University of Yangon, for the use of URC facilities.

.

ABSTRACT

NH_4^+ (1 mol%) doped Nickel Sulphate Heptahydrate, $NiSO_4.7H_2O$ crystals were grown by slow evaporation of aqueous solutions at room temperature. Starting materials of Ammonium Sulphate, $(NH_4)_2SO_4$, $NiSO_4.7H_2O$ salt powders and distilled-water were used to grow the crystals. Structural analysis of the crystal was investigated by XRD method. Temperature dependent electrical conductivity and dielectrics of the crystal were investigated in the temperature range of 300 K – 543 K by using PC-based temperature controller FOTEK MT-20 to study the high temperature phases and to determine the dehydration temperature ($T_{dehydration}$) of the crystal. TG-DTA method was used to formulate the high temperature phases and to conform the dehydration temperature of the sample.

LIST OF FIGURES

LIST OF TABLES

CHAPTER I

INTRODUCTION

The number and variety of scientific and technologically important materials have increased tremendously in recent years. Rare earth elements have an important role in this development and they have their importance for their luminescent, photo conductive, photo refractive, super conducting, laser action and magnetic properties. Along with other (ceramic, glassy) forms of condensed matter, single crystalline materials were basic to fundamental studies of many properties which finally have found widespread applications in optical and other technologies: Dielectric laser and frequency converting crystals emerged from synthetic work in materials physics and efforts in the growth of bulk crystals. Although it is commonly recognized that knowledge on crystal growth and corresponding industrial technologies are indispensable for today's key applications [2, 8].

Ionic conduction of a material depends on the presence of vacant sites into which ions can move. In the absence of a field, thermal vibrations proportional to kT cause ions and vacancies to exchange sites. Heating a crystal increases the vigor of atomic vibrations until the atoms hit one another hard enough to make spaces in which they can move past one another. Then, the crystal melts. At a higher temperature, the molecules vibrate more rapidly and move further away from each other (i.e. slight increase in volume of the solids). Very strong forces hold the molecules together, allowing them to move only slightly apart from each other. Then we can see only very small expansions in solids. Hence, the most solids expand but its expansion is the least compared with liquids and gases. When heated a solid, mass of given solid is unchanged while volume is increase (least expansion) and density is decreased [2, 7].

Nickel sulphate, $NiSO_4$ occurs in nature in a hydrated form, such as $NiSO_4.1H_2O$ (monohydrate), $NiSO_4.5H_2O$ (pentahydrate), $NiSO_4.6H_2O$ (hexahydrate) and $NiSO_4.7H_2O$ (heptahydrate), as several minerals, including morenosite and retgersite. It is used in such applications as nickel plating, the blackening of zinc and brass, and as a mordant in dyeing and printing fabrics. The crystalline hexahydrate, for example, form is

found in two known phases: α-phase: blue to blue-green tetragonal crystals β-phase: green transparent crystals (stable at 40°C). The α to β phase transition occurs at 53.3°C. Nickel Sulphate Hexahydrate, $NiSO_4.6H_2O$ is a water soluble salt which forms hexahydrate (six water) molecules. It is a green colour [4, 20, 22].

Several research workers have carried out much work on mixed crystals of cubic systems. But, very limited studies have been done on orthorhombic systems. Crystal of $NiSO_4.7H_2O$ is orthorhombic with a tetra (Z = 4) molecular unit cell of dimensions *a* = 11.86 Å, *b* = 12.08 Å and *c* = 6.86 Å with the space group of $P_{2_12_12_1}$. It is isomorphous with $MgSO_4.7H_2O$, $ZnSO_4.7H_2O$ and $NiCrO_4.7H_2O$ [4, 20].

In the present work, crystals of NH_4^+(1 mol%) doped $NiSO_4.7H_2O$ were grown and characterized by XRD and temperature dependent electrical conductivity measurements to study the structural and temperature dependent electrical properties of the crystal. TG-DTA method was used to conform the dehydration temperature of the crystal.

CHAPTER II

ELECTRICAL CONDUCTION AND DIELECTRIC BEHAVIOUR OF IONIC CRYSTALS

Ion motion in solids is a very interesting and challenging problem in condensed matter science. Solids come in a variety of structures and forms: single crystalline, polycrystalline (several polymorphs are possible) and glassy. Accordingly, the potential landscape in which the ions move changes remarkably across this gamut. Even within a given solid, temperature and excitation frequencies can trigger a whole range of ion dynamic phenomena. Furthermore, the frequency dependent conductivity of several of these complex systems exhibits universal behaviour. This chapter focuses on conduction mechanism and dielectric behaviour of ionic crystals [2, 10].

2.1 Ionic Conductivity σ_i

Ionic conductivity caused by the motion of ions in an ionic insulating crystal is called ionic conductivity. In a perfect crystal the ions are bound to each other with no freedom of motion. But under certain circumstances the thermal energy at room temperature is sufficient to release a few ions. These ions move through the crystal in a random fashion by hopping over to the various defects centers in the structure. The ion cannot move if the structure is free from defects and so defects are essential for ionic in crystalline solids. Hence ionic conductivity is an important factor for in the investigation of defects. Ionic motion is possible in diffusion and also by an applied electric field.

Ionic conductivity, σ_i, arises when an electric field, E, is applied to an ionic solid. A current density, J, developed in the material is given by

$$J = \sigma_i E \tag{2.1}$$

σ_i is related to mobile ion density N, the mobile ion charge (Ze) and the velocity of the mobile ion per unit electric field or ion mobility, μ.

$$\sigma_i = N(Ze)\mu \tag{2.2}$$

Ion mobility changes with temperature as

$$\mu = \mu_0 \exp(-E_a/kT). \tag{2.3}$$

Thus

$$\sigma = \sigma_0 \exp(-E_a/kT), \quad (2.4)$$

where

$$\sigma_0 = NZe\mu_0. \quad (2.5)$$

E_a is the electrostatic energy barrier that the ion has to overcome in order to hop from one site to another in the crystal/material. Ionic conductivity of a crystal is zero at absolute zero. A non-zero ionic conductivity at a non-zero temperature is the result of defects in a crystal.

2.2 Conduction in Ionic Solids

Crystals contain two major categories of defect: "point" defects and "line" defects. Point defects occur where atoms are missing (vacancies) or occupy the interstices between normal sites (interstitials); "foreign" atoms are also point defects. Line defects, or dislocations, are spatially extensive and involve disturbance of the periodicity or the lattice.

Although dislocations have a significant effect on some of the important properties of ionic and/or hydrogen-boded crystals, especially those depending on matter transport. Schottky defects consist of unoccupied anion and cation sites. A stoichiometric crystalline oxide having Schottky disorder alone contains charge-equivalent numbers of anion and cation vacancies. A Frenkel defect is a misplaced ion, and so a crystal having only Frenkel disorder contains the same concentrations of interstitial ions and corresponding vacant sites. Frenkel defects depend on the existence in a crystal lattice of empty spaces that can accommodate displaced ions.

The equilibrium concentrations of point defects can be derived on the basic of statistical mechanics and the results are identical to those obtained by a less fundamental quasi-chemical approach in which the defects are treated as reacting chemical species obeying the law of mass action. The letter, and simpler, approach is the one widely followed.

The equilibrium concentrations of defects in a simple binary oxide MO are given by

$$n_S \approx N \exp(-\frac{\Delta H_S}{2kT})$$
$$n_F \approx (NN')^{1/2} \exp(-\frac{\Delta H_F}{2kT}) \quad (2.6)$$

where n_S and n_F are the Schottky and Frenkel defect concentrations respectively and ΔH_S and ΔH_F are the enthalpy changes accompanying the formation of the associated defects (cation vacancy + anion vacancy and ion vacancy + interstitial ion); N is the concentration of anions or cations and N' is the concentration of available interstitial sites.

2.3 Charge Transport Parameters

If a material containing a density, n, of mobile charge carriers, each carrying a charge Q, is situated in an electric field E, the charge carriers experience a force causing them to accelerate but, because of interaction with the lattice owing to thermal motion of the atoms or to defects, they quickly reach a terminal velocity, referred to as their drift velocity v as shown in Fig 2.1. All the carriers contained in a prism of cross section A, and length v will move through its end face in unit time. The current density j will therefore be given by

$$j = n\,Q\,v \quad (2.7)$$

If the drift velocity of the charges is proportional to the force acting on them, then

$$v = \mu E \quad (3.8)$$

where μ is the mobility, which is defined as the drift velocity per unit electric field. It follows from above equations

$$j = n\,Q\,\mu\,E \quad (3.9)$$

For materials for which $n\,Q\,\mu$ is constant at constant temperature, this is a statement of Ohm's law:

$$j = \sigma E \quad (2.10)$$

where $\sigma = n\,Q\mu$, is the conductivity of the material.

The resistivity ρ, like the conductivity, is a material property and the two are simply related by $\rho = 1 / \sigma$. In practice it is often the conductive or resistive characteristics of a

specimen of uniform section A and length l which are relevant. The resistance R, conductance G and specimen dimensions are related as follows:

$$R = G^{-1} = \rho l / A \quad (2.11)$$

$$G = R^{-1} = \sigma A / l \quad (2.12)$$

The electrical behaviour of solids depends very much on whether the charge carriers are electrons, ions or a combination of both. The charge transport characteristics of the various types of material so that those of ionic crystal can be seen in proper perspective. Fig 2.2 shows the room temperature values of conductivity characteristic of broad categories of material together with typical dependences of conductivity on temperature. The large difference between the room temperature values of conductivity for the metallic and insulating classes of material, which span probably 30 orders of magnitude at room temperature.

2.4 Ionic Conduction in Crystals

Ionic conduction depends on the presence of vacant sites into which ions can move. In the absence of a field, thermal vibrations proportional to kT cause ions and vacancies to exchange sites. Features that contribute to ionic mobility are small charge, small size and lattice geometry. A highly charged ion will polarize, and be polarized by, the ions of opposite charge as it moves past them, and this will increase the height of the energy barrier that inhibits a change of site. The movement of large ion will be hindered in a similar way by the interaction of its outer electrons with those of the ions it must pass between in order to reach a new site. Some structures may provide channels which give ions space for movement.

The presence of vacant sites assists conduction since it offers the possibility of ions moving from neighbouring sites into a vacancy which, in consequence, moves in the opposite direction to the ions as shown in Fig 2.3. This is particularly likely in the case of the oxygen lattice since the smaller cations do not present large energy barriers impeding the process. However, the cations usually have to pass is

part of the Schottky defect, then n_v / n_S and hence, we obtain

$$j = \frac{A}{T} E \exp(-\frac{\Delta H_S}{2kT}) \exp(-\frac{E_j}{kT}) = \sigma E \qquad (2.13)$$

or

$$\sigma = \frac{A}{T} \exp\{-\frac{1}{kT}(E_j + \frac{\Delta H_S}{2})\}. \qquad (2.14)$$

Because the temperature dependence of σ is dominated by the exponential term, the expression for conductivity is frequently written

$$\sigma = \sigma_0 \exp(-\frac{E_i}{kT}) \qquad (2.15)$$

in which $E_i = E_j + \Delta H_S /2$ is an activation energy and σ_0 is regarded as temperature independent or slope or pre-exponential function.

Vacancies might also be introduced into the crystal extrinsically by the addition of impurities. Under these circumstances, and doping upon the dopant level and the temperature, the concentration of extrinsic defects might be orders of magnitude greater than that of the intrinsic vacancies and independent of temperature. The $\sigma(T)$ relationship would there be as shown in Fig 2.4 where the steep slope in the high-temperature (intrinsic) regime reflects the energy E_i required both to create and to move defects, and the shallower slope in the lower-temperature (extrinsic) regime reflects the energy E_j required only to move defects only.

In the absence of an electric field the charged vacancy migrates randomly, and its mobility depends on temperature. Because the crystal is highly ionic in character the barrier is electrostatic potential energy "well". It is clear from Fig 2.3 that in the simplified one-dimensional representation and in the absence of an electric field the vacancy would have equal probability of jumping to the right or to the left, because the barrier height E_j is the same in both directions. However, when an electric field E is imposed the barrier heights are no longer equal, and the jump probability is higher for the jump across the lower barrier (in Fig 2.3, to the right) of height, $E_j - \Delta E_j$ where $\Delta E_j = e\,E\,a/2$.

Since we know the bias in jump probability in one direction, it is not difficult to arrive at the following expression for the current density:

$$j = \frac{n_v A}{N T} E \exp(-\frac{E_j}{k T}) \qquad (2.16)$$

in which n_v/N is the fraction of positive ion sites that are vacant and A is a constant describing the vibrational state of the crystal.

2.5 Dielectric Behavior

Electrical insulators are also known as dielectrics. Most ionic solids and molecular solids are insulators because of the negligible concentration of conduction electrons or holes [2, 14].

Consider two metal (conductor) plates connected to the two ends of a battery of voltage V (Fig 2.5). Assuming the electrical resistance of the connecting wires is negligible, the potential between the two metal plates is V. Assume that the medium between the plates is a vacuum.

There are a lot of conduction electrons in the metal plates and metal wires. The positive end of the battery attracts conduction electrons, making the left plate positively charged (charge = +Q). The negative end of the battery repels conduction electrons, making the right plate negatively charged (charge = –Q). Let the area of each plate be A. the magnitude of charge per unit area of each plate is known as the "charge density" (D_0).

$$D_0 = \frac{Q}{A}$$

The electric field E between the plates is given by

$$E = \frac{V}{d}$$

where d is the separation of the plates. When E = 0, $D_0 = 0$. In fact, D is proportional to E. Let the proportionality constant be ε_0. Then

$$D_0 = \varepsilon_0 E \qquad (2.17)$$

ε_0 is called the "permittivity of free space." It is a universal constant.

($\varepsilon_0 = 8.854 \times 10^{-12}$ C V^{-1} m^{-1})

Eqn (2.17) is known as Gauss's law. Just as D_0 is proportional to E, Q is proportional to V. The plot of Q versus V is a straight line through the origin (Fig 2.6), with

$$\text{Slope} = C_0 = \frac{Q}{V} = \frac{\varepsilon_0 E A}{E d} = \frac{\varepsilon_0 A}{d} \qquad (2.18)$$

C_0 is known as the capacitance (C V^{-1} or F). This is the principle behind a parallel-plate capacitor.

Next, consider that the medium between the two plates is not a vacuum, but an insulator whose center of positive charge and center of negative charge coincide when V = 0. When V > 0, the center of positive charge is shifted toward the negative plate, while the center of negative charge is shifted toward the positive plate. Such displacement of the centers of positive and negative charges is known as "polarization". In the case of a molecular solid with polarized molecules (e.g., HF), the polarization in the molecular solid is due to the preferred orientation of each molecule such that the positive end of the molecule is closer to the negative plate. In the case of an ionic solid, the polarization is due to the slight movement of the cations toward the negative plate, and that of the anions toward the positive plate. In the case of an atomic solid, the polarization is due to the skewing of the electron clouds toward the positive plate.

When polarization occurs, the center of positive charge sucks more electrons to the negative plate, causing the charge on the negative plate to be $-\kappa Q$, where $\kappa > 1$ (Fig 2.7). Similarly, the center of negative charge repels more electrons away from the positive plate, causing the charge on the positive plate to be κQ. κ is a unitless number called the "relative dielectric constant".

The charges in the plates when a vacuum is between the plates are called “free charges” (magnitude = Q on each plate). The extra charges in the plates when an insulator is between the plates are called the “bound charges” (magnitude = $\kappa Q - Q = (\kappa - 1)Q$ on each plate).

When an insulator is between the plates, the charge density is given by

$$D_m = \kappa D_0 = \frac{\kappa Q}{A} \qquad (2.19)$$

Using Eqn (2.17), Eqn (2.19) becomes

$$D_m = \kappa \varepsilon_0 E = \varepsilon E$$

where $\varepsilon = \kappa \varepsilon_0$; ε is known as the dielectric constant, whereas κ is known as the relative dielectric constant. Hence, ε and ε_0 have the same unit.

When an insulator is between the plates, the capacitance is given by

$$C_m = \frac{\kappa Q}{V} = \frac{\kappa \varepsilon_0 E A}{E d} = \frac{\kappa \varepsilon_0 A}{d} = \kappa C_0 \qquad (2.20)$$

From Eqn (2.20), the capacitance is inversely proportional to d, so capacitance measurement provides a way to detect changes in d (i.e., to sense strain).

Dielectric measurement refers to measurement of the relative dielectric constant κ of a dielectric material. Parallel plate geometry is used because the capacitance increases with plate area. This geometry involves sandwiching the sample between electrical conductor plates, applying a voltage across the parallel plates, and measuring the impedance across the plates.

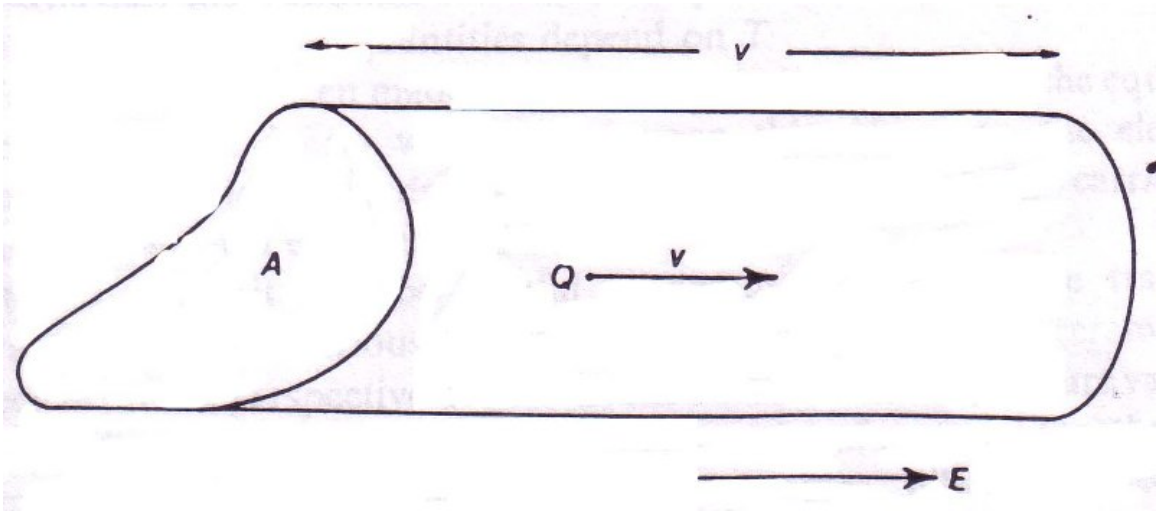

Fig 2.1 Flow of charge in a solid material [2]

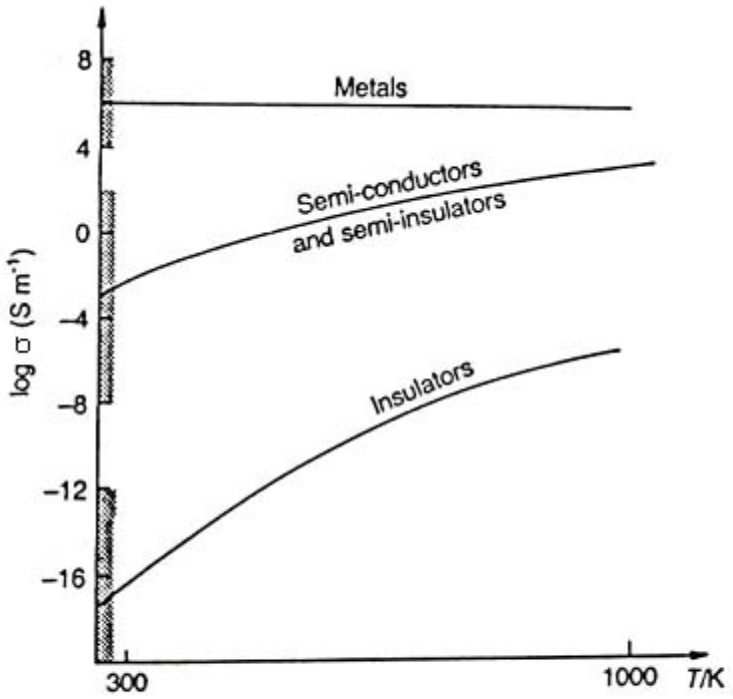

Fig 2.2 Conductivities of various classes of material [2]

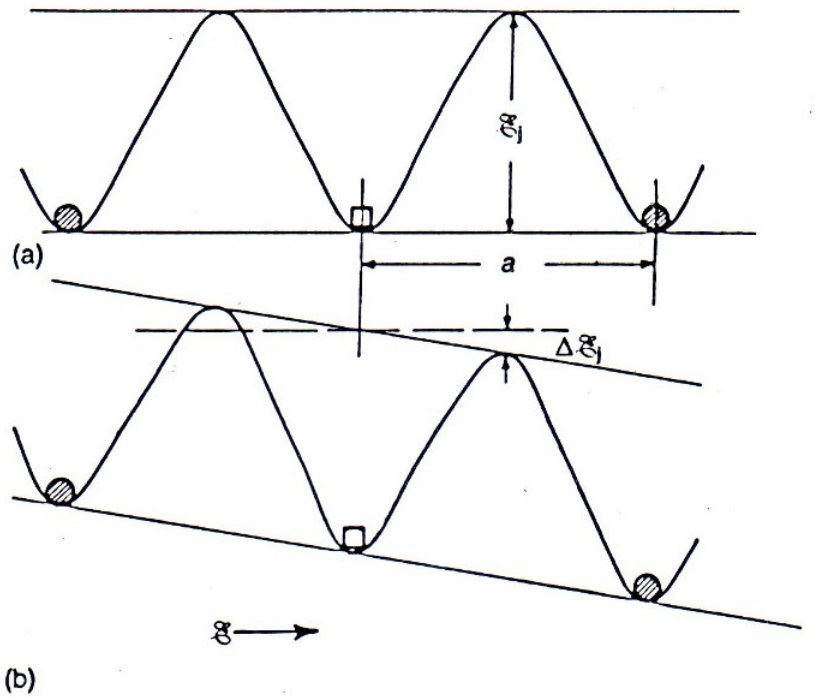

Fig 2.3 Energy barriers to ionic transport in a crystal (a) in the absence of a field and (b) with applied field *E* [10]

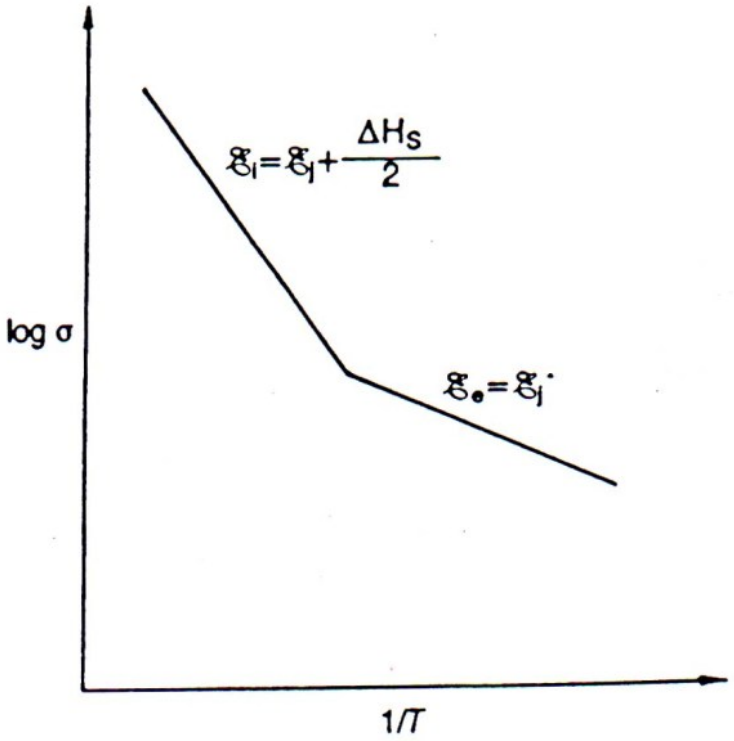

Fig 2.4 Extrinsic and intrinsic regimes in the log σ versus 1/T relation [2]

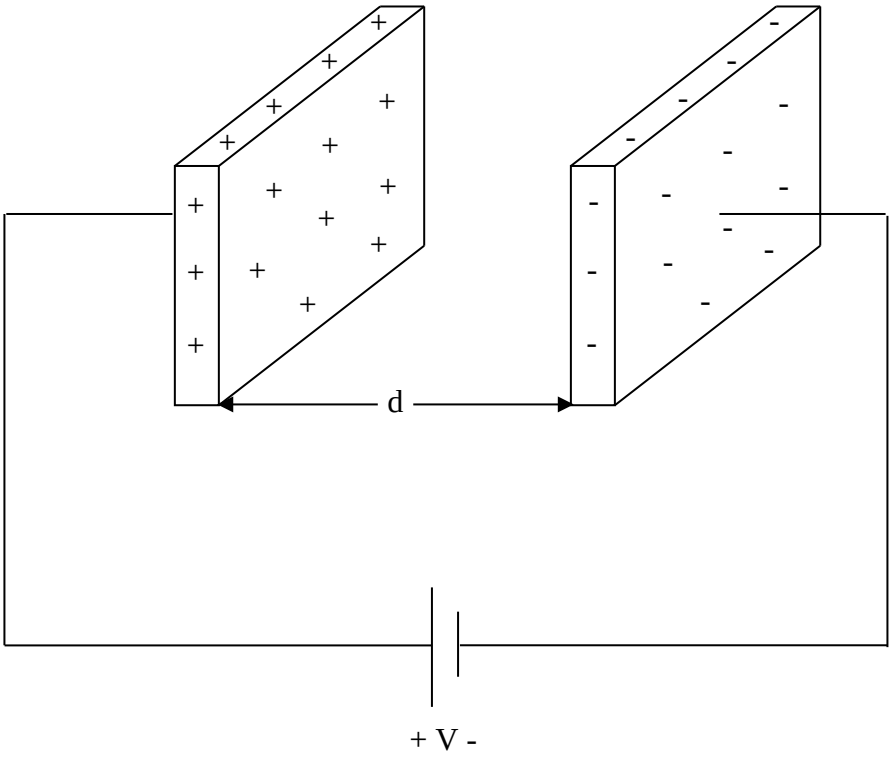

Fig 2.5 A pair of positively charged and negatively charged conductor plates in vacuum [2]

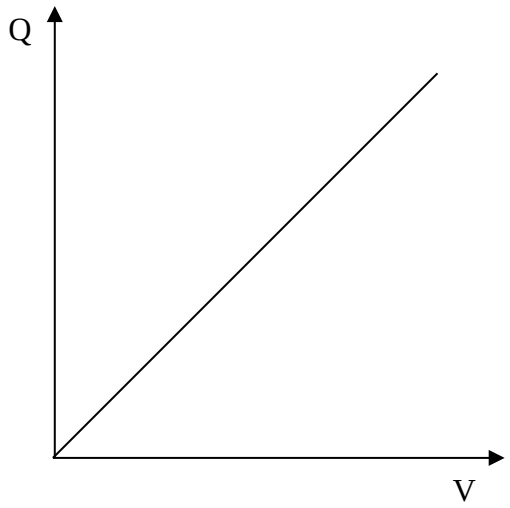

Fig 2.6 Plot of charge Q vs potential V. The slope = $C_0 = \frac{\varepsilon_0 A}{d}$ [2]

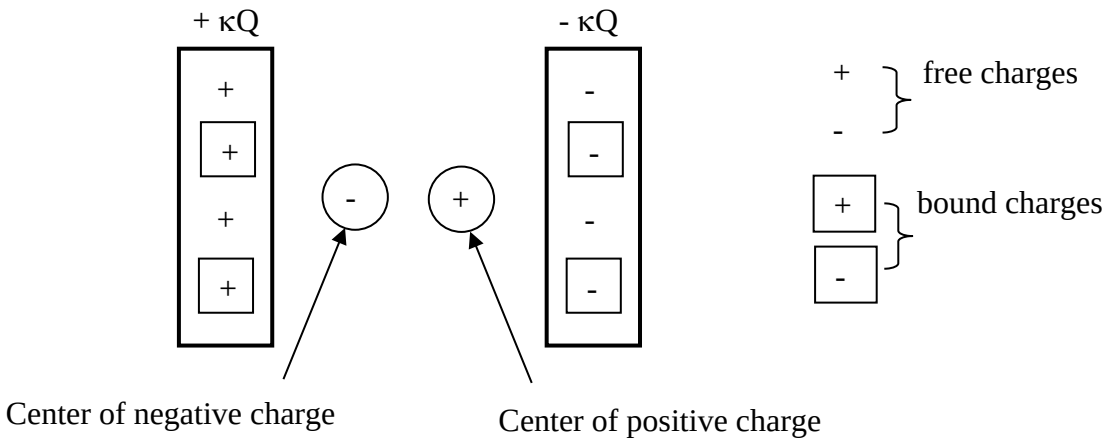

Fig 2.7 A pair of positively charged and negatively charged conductor plates in a medium with relative dielectric constant κ [2]

CHAPTER III

THERMAL ANALYSIS

Thermal properties of materials are important aspects of their behavior. For example, the melting point of a metal will determine its upper use temperature as well as establish what conditions are needed to process it [1]. Crystalline materials possess a melting temperature above which the ordered solid melts into a liquid. Above this temperature the chemical potential of the liquid phase is lower than that of the solid (i.e. in the melt, $\mu_{liq} < \mu_{sol}$ but is reversed in the solid state, $\mu_{sol} < \mu_{liq}$) [1, 2]. There also exist many types of materials with multiple crystalline phases (for example, iron has several crystal forms, the presence of which depends on temperature). Other kinds of materials have ordered liquid phases, that is, they retain some of the translational order found in a crystal even though they might be in a molten state. Such materials are known as liquid crystals. Transitions to these phases of reduced order (less than a crystal, but more than a liquid) are detected on a DSC (Differential Scanning Calorimetry) by a peak of similar form to a melting peak, but are of smaller size.

3.1 Thermogravimetric Analysis (TGA)

Thermogravimetry is a technique for measuring the change in weight of a substance as a function of temperature or time. The results usually appear as a continuous chart record; a schematic typical single step decomposition reaction is shown in Fig 3.1. The sample, usually a few milligram (mg) in weight, is heated at a constant rate, typically 1 to 20°C min^{-1}, and has a constant weight W_i, until its begins to decompose at temperature T_i. Under condition of dynamic heating, decomposition usually takes place over a range of temperatures, T_i to T_f, and a second constant rate of plateau is then observed above T_f, which corresponds to the weight of the residue W_f. The weight W_i, W_f and the difference in weight ΔW are fundamental properties of the sample and can be used for quantitative calculations of compositional changes, etc. By contrast, the temperatures T_i to T_f depend on variables such as heating rate, the nature of the solid (e.g., its particle size) and the atmosphere above the sample. The effect of atmosphere can be dramatic, as shown

in Fig 3.2 for the decomposition of $CaCO_3$; in vacuum, the decomposition is complete by ~ 500°C, but in CO_2 at one atmosphere pressure, decomposition does not even commence until above 900°C. T_i and T_f pertain to the particular experimental conditions, and do not necessarily represent equilibrium decomposition temperatures.

3.2 Differential Thermal Analysis (DTA)

Differential Thermal Analysis (DTA) is a technique for identifying and quantitatively analyzing the chemical composition and physical characteristics of substances by observing the thermal behaviour of a sample as it is heated. The technique is based on the fact that as a substance is heated, it undergoes reactions and phase changes that involves absorption or emission of heat. In DTA the temperature of the test material is measured relative to that of an adjacent inert material. A thermocouple imbedded in the test piece and another in the inert material are connected so that any differential temperatures generated during the heating cycle are graphically recorded as a series of peaks on a moving chart. The amount of heat involved and temperature at which these changes take place are characteristic of individual elements or compounds; identification of a substance, therefore, is accomplished by comparing DTA curves obtained from the unknown with those of known elements or compounds. Moreover, the amount of a substance present in a composite sample will be related to the area under the peaks in the graph, and this amount can be determined by comparing the area of a characteristic peak with areas from a series of standard samples analyzed under identical conditions. The DTA technique is widely used for identifying minerals and mineral mixtures.

The temperature changes occurring during these chemical or physical changes are detected by a differential method, such as is illustrated in Fig 3.3. If the sample and reference temperatures are T_s and T_r, respectively, then the difference in temperature, T_s - T_r , is the function recorded. Perhaps a better name for this technique would be *differential thermometry*; the term “differential thermal
analysis” implies that it has something to do with analysis, which, as with any other analytical technique, may or may not be the case. In *thermal analysis*, the temperature of the sample, T_s, is recorded as a function of time, and a heating or cooling curve is

recorded. Small temperature changes occurring in the sample are generally not detected by this method. In the *differential* technique, since the detection thermocouples are opposed to each other, small differences between T_s and T_r can be detected with the appropriate voltage amplification devices. Thus, small samples (down to several μg or mg in mass) may be employed and are, as a matter of fact, more desirable. A comparison between the two techniques is shown in Fig 3.4. In parts (a) and (b), the sample temperature is recorded as a function of time as the system temperature is increased at a linear rate. However, the difference between the curves in (a) and (b) is that no enthalpic transition takes place in the sample in (a), while in (b) exothermic and endothermic changes occur. Since no other temperature changes take place in the sample in (a), no deviation from the linear temperature rise is detected in the sample temperature. However, in (b), deviations occur at the procedural initial reaction temperature, T_i, due to temperature changes are essentially completed at T_f and the temperature of the sample returns to that of the system. In the curves in (c), the difference in temperature, T_s-T_r, is recorded as a function of system temperature, T. At T_i, the curve deviates from a horizontal position to form a peak in either the upward or the downward direction, depending upon the enthalpic change. The completion of the reaction temperature, T_f, does not occur at the maximum or minimum of its curve but rather at the high-temperature side of the peak. Its exact position depends upon the instrumental arrangement. Thus, in the differential method, small temperature changes can be easily detected while the peak area is proportional to the enthalpic change ($\pm \Delta H$) and sample mass.

A typical DTA curve is illustrated in Fig 3.5. Four types of transitions are illustrated: (I) second-order transition in which a change in the horizontal base line is detected; (II) or (III) an endothermic curve peak due to a decomposition or dissociation reaction; and (IV) an exothermic curve peak caused by a crystalline phase change.

The number, shape, and position of the various endothermic and exothermic peaks with reference to the temperature may be used as a means for the qualitative identification of the substance under investigation. Also, since the area under the peak is proportional to the heat-change involved, the technique is useful for the semiquantitative or, in some cases, quantitative determination of the heat of reaction. As the heat of reaction is

proportional to the amount of reacting substance, DTA can be used to evaluate quantitatively the amount of substance present if the heat of reaction is known. Thus, the technique finds much use in the qualitative and semiquantitative identification of organic and inorganic compounds, clays, metals, minerals, fats and oils, polymeric materials, coal and shales, wood, and other substances. It can also be used to determine the radiation damage of certain polymeric materials, the amount of radiation energy stored in various minerals, heats of absorption, effectiveness of catalytic materials, heats of polymerization, and others. Quantitatively, it can be used for the determination of a reactive component in a mixture, or the heat of reaction involved in physical and chemical changes.

3.3 Factors Affecting the DTA Curve

Differential thermal analysis, since it is a dynamic temperature technique, has a large number of factors which can affect the resulting experimental curves. These factors, which are similar to those discussed in thermogravimetry, are more numerous in DTA and can have a more pronounced effect on the curve. If the DTA curve is used for qualitative purposes, the shape, position, and number of endothermic and exothermic curve peaks is important. By a simple change of conditions, say heating rate or furnace atmosphere, the positions (with reference to the T axis) will be changed, and perhaps the number of curve peaks as well. Changing from nitrogen to an oxygen atmosphere can create additional exothermic peaks. For quantitative studies, the area enclosed by the curve peak is of great interest, so the effect of the experimental parameters on the area must be known. When DTA is used for specific heat measurements, the baseline deviations become important and such conditions as particle size of sample and diluent, system symmetry, sample packing, and so on must be taken into account if accurate and reproducible results are to be obtained. A generalized DTA curve which will be used for purpose of this discussion is shown in Fig 3.6. An endothermic peak is illustrated in which A is the pretransition (or prereaction) base line, B is the post-transition base line, T_i is the procedural initial deviation temperature which the instrument can detect, ΔT_{min} is the procedural peak minimum temperature, and T_f is the procedural final temperature of the curve peak. For the temperature axis, T_n is the temperature of the reference (T_r),

sample (T_s), or furnace (external) (T_e). The *Y* axis is that of the differential temperature, $T_s - T_r$ or ΔT.

As with the technique of thermogravimetry, the DTA curve is dependent upon two general categories of variables: (a) instrumental factors and (b) sample characteristics. The former category includes

(a) Instrumental factors,
  (1) furnace size and shape,
  (2) sample-holder material,
  (3) sample-holder geometry,
  (4) wire and bead size of thermocouple junction,
  (5) heating rate,
  (6) speed and response of recording instrument,
  (7) thermocouple location in sample,

While the latter consists of

(b) Sample Characteristics
  (1) particle size,
  (2) thermal conductivity,
  (3) heat capacity,
  (4) packing density,
  (5) swelling or shrinkage of sample,
  (6) amount of sample,
  (7) effect of diluent,
  (8) degree of crystallinity.

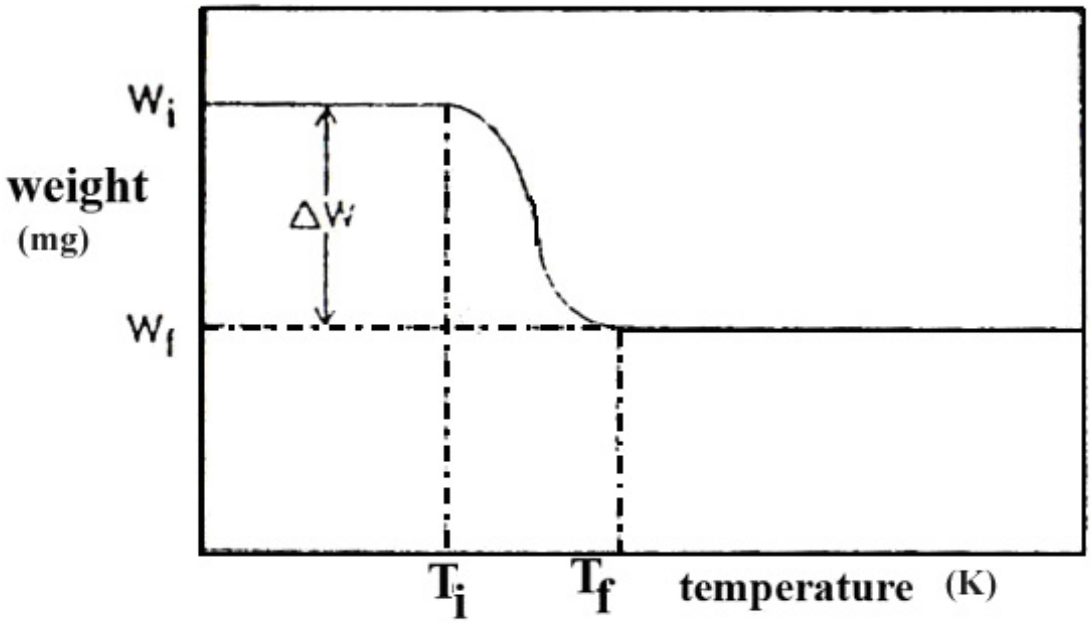

Fig 3.1 A schematic typical single step decomposition reaction

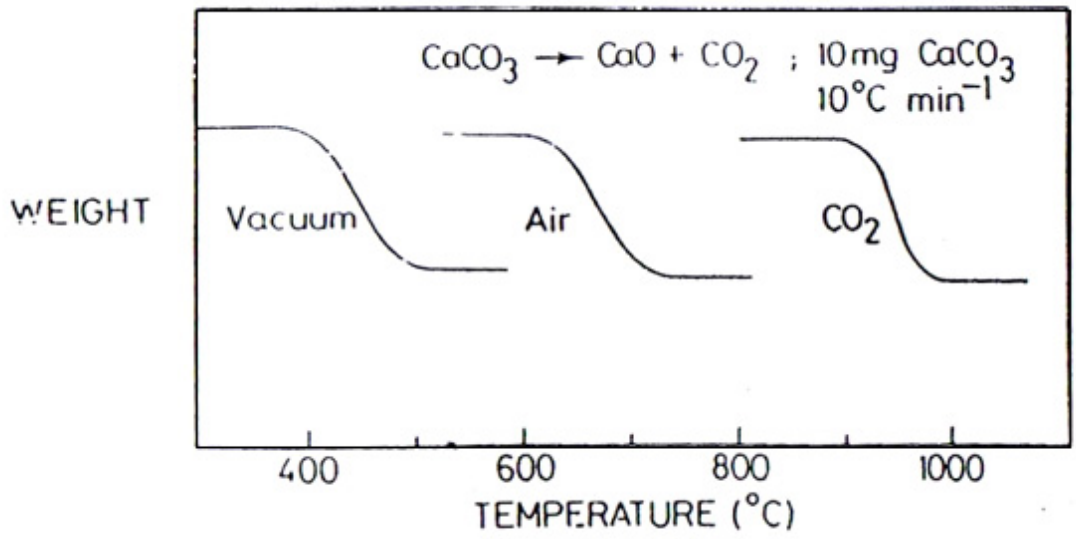

Fig 3.2 Decomposition of $CaCO_3$ in different atmospheres

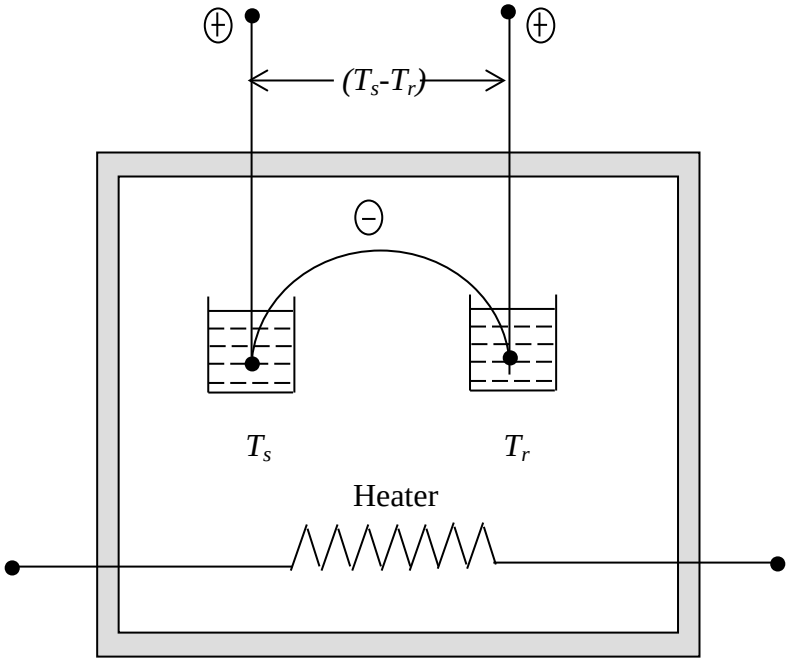

Fig 3.3 Basic DTA system

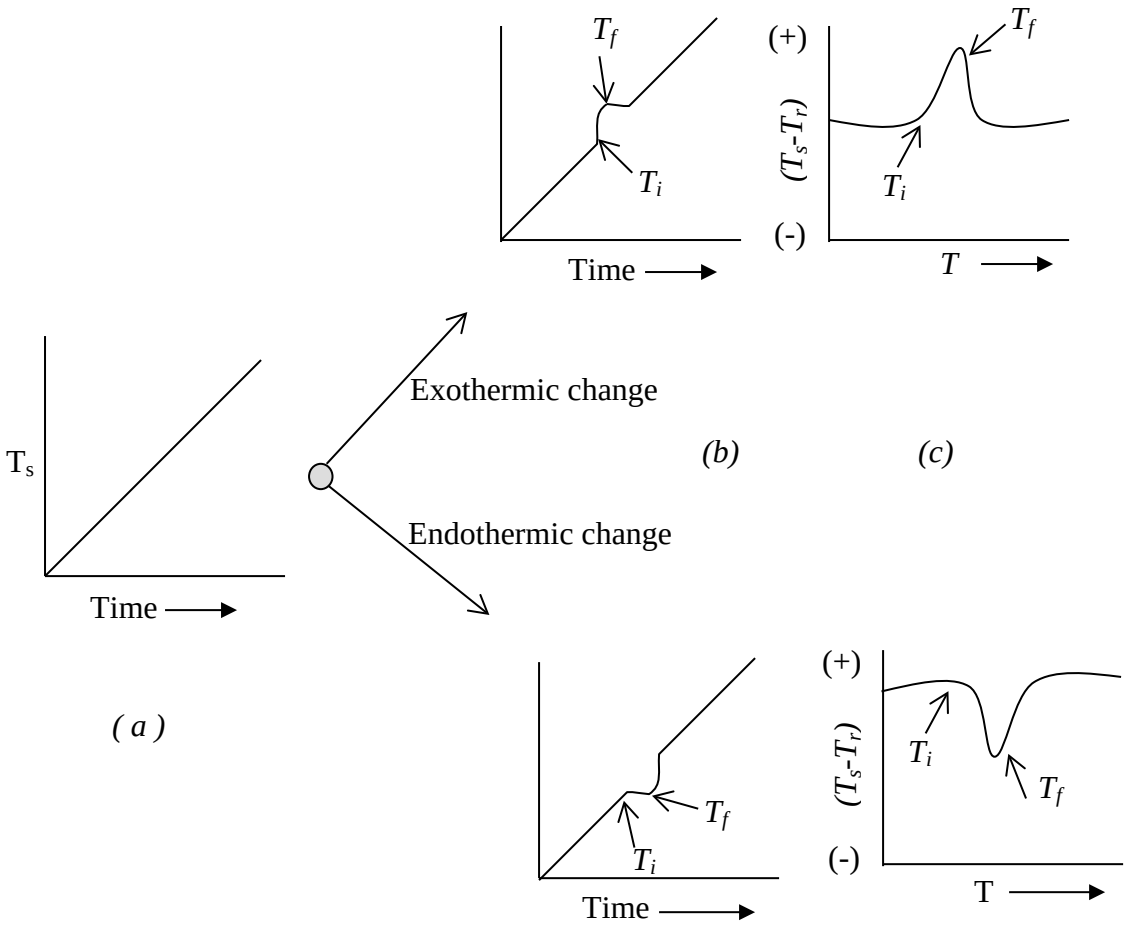

Fig 3.4 Comparison between thermal analysis and differential thermal analysis

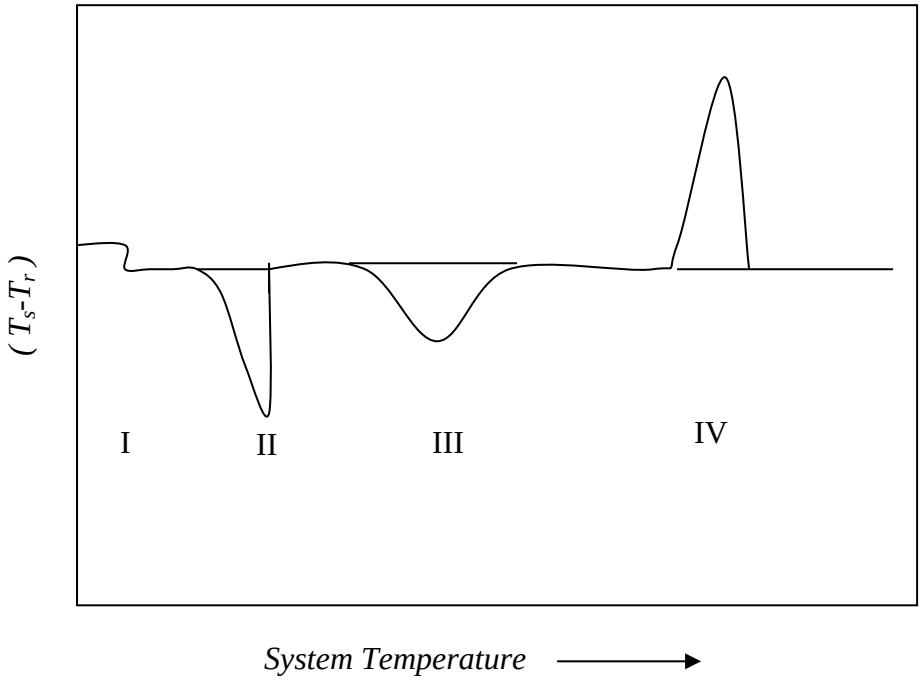

Fig 3.5 Typical DTA curve

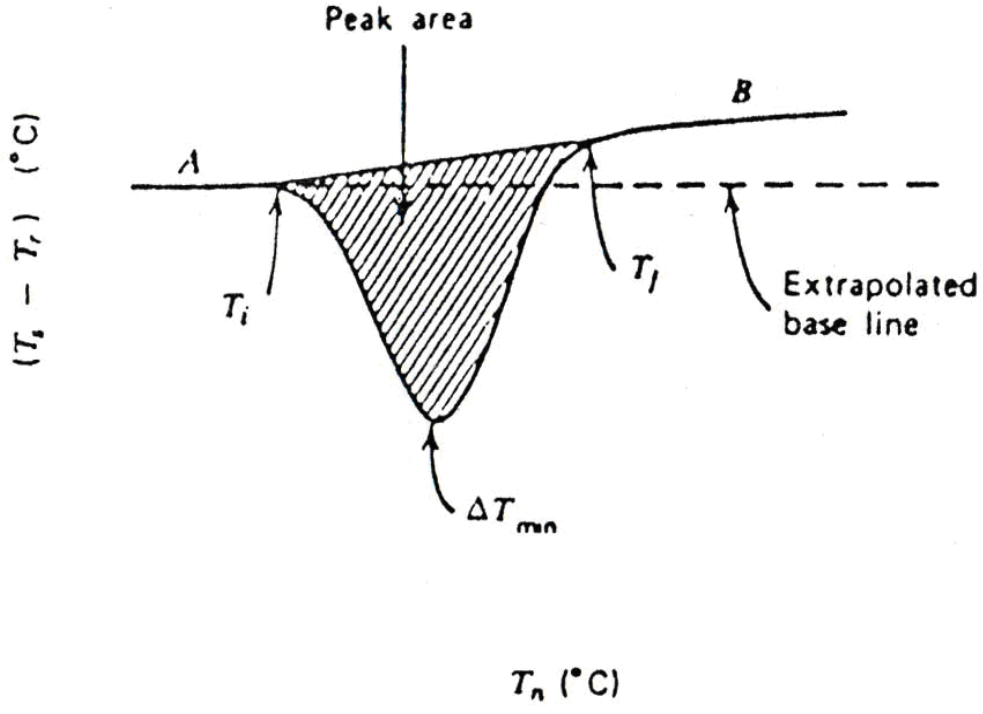

Fig 3.6 Generalized DTA curve

CHAPTER IV

CRYSTAL GROWTH AND MEASUREMENTS

Growth of $NH_4^+/NiSO_4.7H_2O$ crystal and its characteristic measurements are essential parts of the present experimental work. Some details will be described because they are important in practice based on doing experiment in this work and also in the related fields.

4.1 Growth of NH_4^+(1 mol%) doped $NiSO_4.7H_2O$ Crystal

Crystals of Ammonium, NH_4^+(1 mol%) doped Nickel Sulphate Heptahydrate, $NiSO_4.7H_2O$ were grown by slow evaporation method from aqueous solutions at room temperature. Starting materials of Ammonium Sulphate, $(NH_4)_2SO_4$ and Nickel Sulphate Heptahydrate, $NiSO_4.7H_2O$ salt powders with molar ratio were used to grow and synthesis for the crystals. Transparent and homogeneous crystals were selected for measurements [4, 7]. At room temperature, $NH_4^+/NiSO_4.7H_2O$ crystal is green in colour. Photograph showing the as-grown $NH_4^+/NiSO_4.7H_2O$ crystal is shown in Fig 4.1.

4.2 X-Ray Diffraction Measurement

X-ray diffractometry was mainly used for identification and qualification of crystals by their diffraction patterns. The X-ray diffraction measurements were carried out by using RIGAKU MULTIFLEX X-ray powder diffractometer at URC,
Yangon University. Photograph showing the RIGAKU MULTIFLEX X-ray powder diffractometer is shown in Fig 4.2. The X-ray diffractometry consists of three basic parts: a source of radiation, consisting of (1) X-ray tube and high voltage generator, (2) the detector and counting equipment, and (3) the diffractometer.

The powder sample of $NH_4^+/NiSO_4.7H_2O$ crystal was placed at the center of the goniometer. The samples were scanned through an angle 2θ from 10° to 70°. The surface of the sample was radiated by X-ray beam from Cu fine focus tube.
The applied voltage and current were maintained at 40 kV and 40 mA. The diffracted X-ray beams entered the detector and then recorded. The recording scan speed was 4°/min. Each diffracted ray is recorded as a peak. The peak heights are roughly proportional to the

X-rays intensity. The diffraction patterns of specimens were identified by using Material Data Inc. data book. The initial "d" spacing was determined using a second derivative peak search algorithm, followed by careful editing of the raw data to improve the position accuracy and to resolve ambiguous lines. The "d" values were determined using the CuK_α radiation with wavelength of 1.54056Å. The lattice parameters can be examined by using the following equation [10, 19].

$$\frac{1}{d^2}=\frac{h^2}{a^2}+\frac{k^2}{b^2}+\frac{l^2}{c^2}=\frac{4\sin^2\theta}{\lambda^2} \qquad (4.1)$$

where d is interplanar spacing (Å), *a, b* and *c* are lattice parameters (Å) of the unit cell, (*h k l*) are Miller indices, θ is diffraction angle (°) and λ is wavelength of incident X-ray (Å).

The experimental conditions are as follows:

Tube Voltage	: 40 kV, 40 mA
Target	: Cu
Filter	: Ni
Wavelength	: 1.54056 Å (CuK_α-radiation)
Scan Speed	: 4°/min
2θ range	: 10° - 70°

4.3 FTIR Spectroscopic Measurement

There are, in general, several types of motion that a molecule may undergo. First, the molecule as a whole may move through space in some arbitrary direction and with a particular velocity. This type of motion is called translational motion and with it we associate the translational motion of the molecule. Second, the molecule may rotate about some internal axis. Again, any such axis may be resolved into components along the x, y, and z axes of a Cartesian coordinate system, so that any rotation of the molecule may be resolved into three mutually perpendicular components. Finally, the molecule may vibrate. Each of the vibrational motions of a molecule occurs with a certain frequency, which is characteristic of the molecule and of the particular vibration [8, 14].

The frequency of light required to cause a transition for a particular vibration is equal to the frequency of that vibration, so that we may measure the vibrational frequencies by measuring the frequencies of light which are absorbed by the molecule. As it happens, light of this wavelength lies in the so-called infrared region of the spectrum. IR spectroscopy, then, deals with transitions between vibrational energy levels in molecules, and is therefore also called vibrational spectroscopy. An IR spectrum is generally displayed as a plot of the energy of the infrared radiation versus the percent of light transmitted by the compound.

Most of the solid samples absorb IR radiation or IR radiation cannot transmit most of the solid samples. Thus we must choose the window materials of IR radiation. Moreover, the material must be transparent to the incident IR radiation and therefore alkali halides are normally used in transmission method. The most commonly used alkali halide is potassium bromide (KBr), which is completely transparent in the middle IR region because KBr is an inert, infrared transparent material, and acts as a support and a diluent for the sample.

FTIR transmission spectrum of $NH_4^+/NiSO_4.7H_2O$ crystal was observed by SHIMADZU FTIR-8400 spectrophotometer using Potassium Bromide, KBr pellet method. Photograph

of the SHIMADZU FTIR-8400 spectrophotometer is shown in Fig 4.3. Experimental conditions were as follows:

wavenumber range : 400 cm^{-1} – 4000 cm^{-1}

method : KBr pellet method

measurement mode : %T

measuring time : 60 s.

4.4 FT-Raman Spectroscopic Measurement

Raman spectroscopy is based on the absorption of photons of a specific frequency followed by scattering at a higher or lower frequency. The modification of the scattered photons results from the incident photons either gaining energy from or losing energy to the vibrational and rotational motion of the molecule. Quantitatively, a sample (solid, liquid, or gas) is irradiated with a source frequency ν_0 and the scattered radiation will be of frequency $\nu_0 \pm \nu_i$, where ν_i is the frequency corresponding to a vibrational or rotational transition in the molecule. Since molecules exist in a number of different rotational and vibrational states (depending on the temperature), many different values of ν_i are possible. Consequently, the Raman spectra will consist of a large number of scattered lines [12, 21, 24].

FT-Raman spectrum of $NH_4^+/NiSO_4.7H_2O$ crystal was recorded on PC-controlled Perkin Elmer FT-Raman Spectrometer in the Raman shift range of 400 cm^{-1} to 4000 cm^{-1} region. Photograph of the Perkin Elmer FT-Raman Spectrometer is shown in Fig 4.4. In this measurement, the as-grown crystal was first polished with filter-paper to get a smooth and polish surface of the crystal because the sample must be optically transparent and good reflecting surface. The crystal was then place on the sample holder to collect the FT-Raman spectrum. Fig 4.5 shows the vibrational transitions or energy level diagram of IR and Raman effects.

Experimental conditions were as follows:

laser source	: Nd-YAG laser
wavelength	: 1064 nm (invisible laser)
scattering geometry	: 90° (laser source & detector)
measuring time	: 20 s.
Raman shift range	: 400 cm^{-1} – 4000 cm^{-1}

4.5 Sample Preparation and Temperature Dependent Electrical Conductivity Measurement

Temperature dependent resistances and capacitances of $NH_4^+/NiSO_4.7H_2O$ crystal were observed in the temperature range of 300 K (27°C) - 543 K (270°C) by using PC-based temperature controller FOTEK MT-20. The dimensions of the crystal were measured by Digital Vernier Caliper (Taiwan). The dimensions of the crystal were as (1.15 cm in length, 1.10 cm in width, 0.28 cm in thickness).

Firstly, the crystal was fixed on glass plate and silver contacts were made over the sample to ensure good electrical contacts to measure the electrical properties such as resistances that change with temperatures. Of course, the surfaces of the macroscopic or as-grown crystals (sample surfaces) and electrodes (copper plates) are not optically homogeneous. But, in practice, the surfaces of the crystal and electrodes must be homogeneously contacted with each others when the light or temperature dependence measurements of electrical parameters, such as resistance, capacitance and voltage of the samples. Thus, silver paste (electrical and thermal conducting paste) was used to interface or homogeneously contacted between surfaces of crystal and electrodes. Electrical conductivity measurements were made on the crystal in a stainless-steel conductivity cell in which maintained the crystal by a spring-loaded support between copper leads using two polished Cu disc as electrodes (see Fig 4.6). Photograph of the experimental arrangement of temperature dependent electrical conductivity measurement is shown in Fig 4.7.

The temperature sensor of K-type thermocouple (up to 1073 K) was placed near the sample to record real temperatures throughout the measurement. The copper block holder (heater chamber) was heated by using the two of 350W heater coils. Temperature dependent resistances and capacitances of the sample were measured by using FUKE FK9208X digital resistance meter (1 Ω – 2000 MΩ) and WHDZ CM9601A digital Capacitance meter (2 μF – 2000 pF). The electrical conductivity of ionic crystals have been calculated by using the formula

$\sigma = \frac{l}{RA}$ where l is the thickness of the sample (cm), A is the cross-sectional area of the sample (cm^2) and R is the resistance of the sample (Ω) [2, 14].

The value of dielectric constant ε_r have been calculated by using the relation, $\varepsilon_r = \frac{1}{\varepsilon_0}\frac{Ct}{A}$ where C is the capacitance (F), t is the thickness (cm), A is the cross-sectional area (cm^2) of the crystal and ε_0 is the permittivity of free space (8.85×10^{-12} C^2 / Nm^2).

4.6 TG-DTA Measurement

Thermal analysis may be defined as the measurement of physical and chemical properties of materials as a function of temperature. In practice, however, the term thermal analysis is used to cover certain specific properties only. These are enthalpy, heat capacity, mass and coefficient of thermal expansion. Uses of thermal analysis in solid state science are many and varied and include the study of solid state reactions, thermal decompositions and phase transitions and determination of phase diagrams.

Most kinds of solids are “thermally active” in one way or another and may be profitably studied by thermal analysis. The two main thermal analysis techniques are “thermogravimetric analysis” (TGA), which automatically records the change in weight of a sample as a function of either temperature or time, and “differential thermal analysis” (DTA), which measures the difference in temperature, ΔT between a sample and an inert reference material as a function of temperature; DTA therefore detects changes in heat contents [1, 2]. With modern, automatic thermal analysis equipment it is possible to do TGA and DTA using the same instrument; with some models, TGA and DTA may be carried out simultaneously.

The DTA measurement with higher accuracy was carried out along with thermal gravitational analysis (TGA) using Shimadzu’s apparatus DTG-60H as shown in Fig 4.8(a) and the DTA Instrument (built-in DTG-60H) as shown in Fig 4.8(b) [1, 22]. Aluminium (Al) pan was used as the standard sample. All measurements were carried out by heating run under N_2 atmosphere. The speed of heating was chosen at the rate of 20°C/min and kept constant in the respective runs. 3.09 mg mass of the powdered samples of the crystal was used to collect the TG-DTA thermograms.

Experimental conditions were used as follows:

Sample	: $NH_4^+/NiSO_4.7H_2O$ crystal
Mass	: 4.17 mg
Pan	: Al
Atmosphere	: N_2

Flow Rate	: 50 ml/min
Start Temperature	: 30°C
End Temperature	: 600°C
Heating Rate	: 25°C/min

Fig 4.1 Photograph showing the as-grown $NH_4^+/NiSO_4.7H_2O$ crystal

Fig 4.2 Photograph of the RIGAKU MULTIFLEX X-ray Diffractometer

Fig 4.3 Photograph of the SHIMADZU FTIR-8400 Spectrophotometer

Fig 4.4 Photograph of the Perkin Elmer FT-Raman Spectrometer

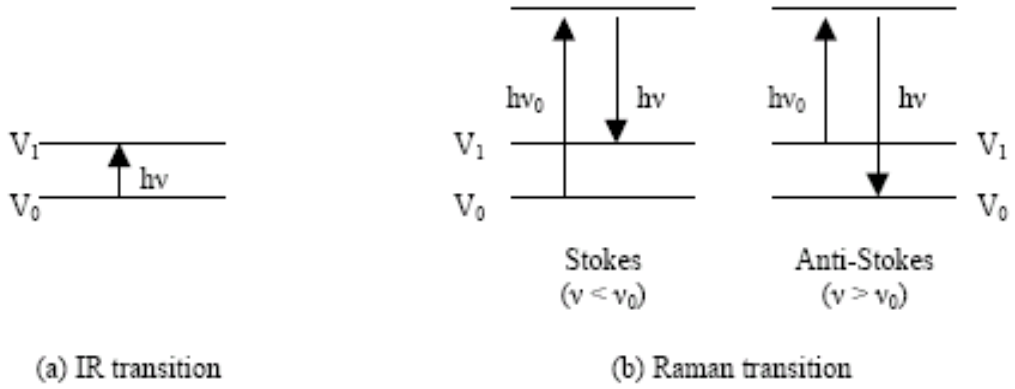

Fig 4.5 Vibrational transitions of IR and Raman effects

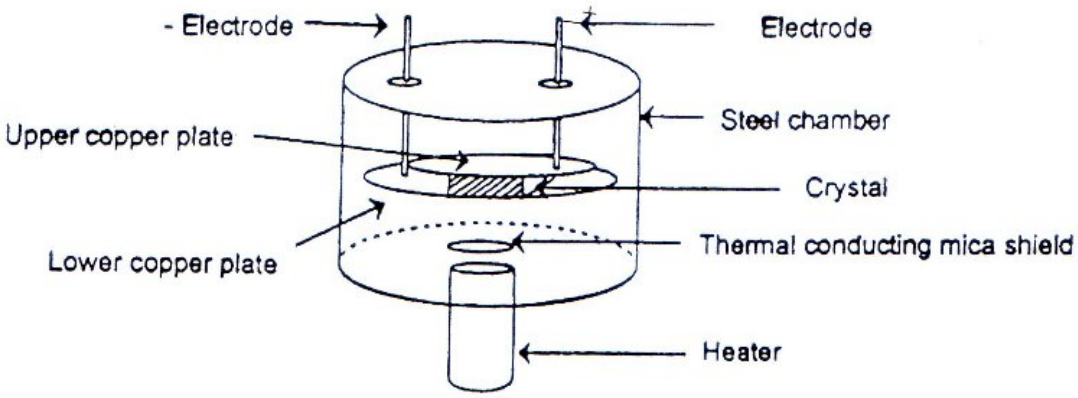

Fig 4.6 Internal setup of sample preparation for the electrical conductivity measurement

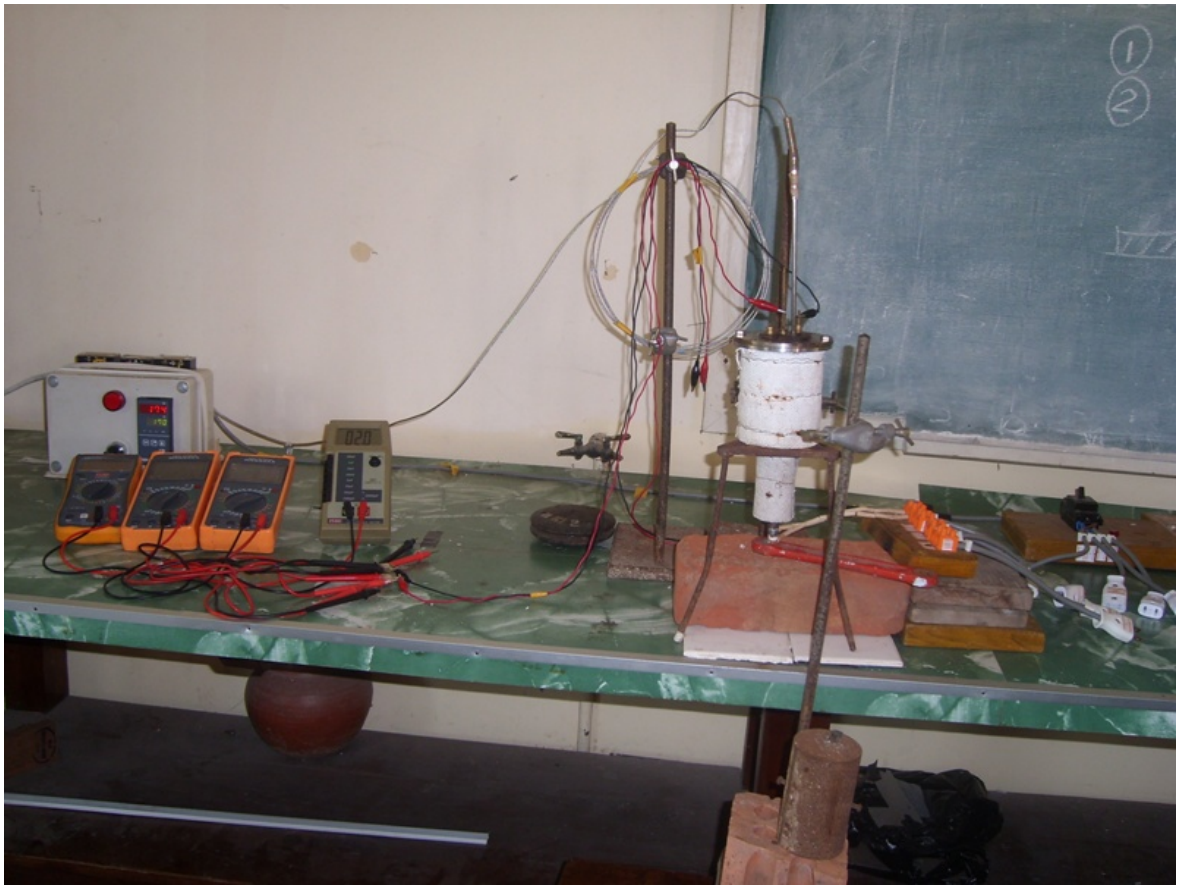

Fig 4.7 Photograph of the experimental setup of temperature dependent conductivity measurement

Fig 4.8(a) Photograph of SHIMADZU DTG-60H Thermal Analyzer

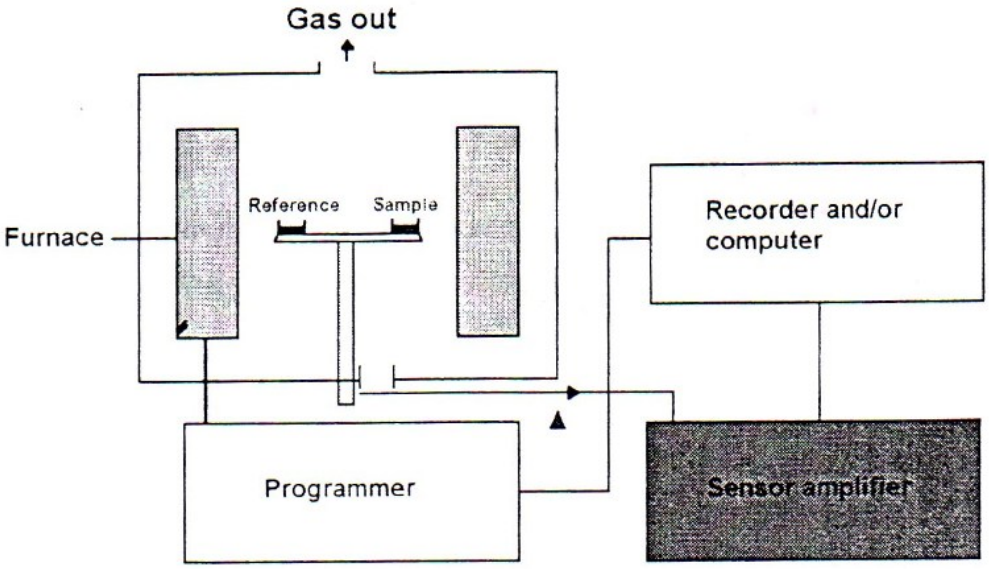

Fig 4.8(b) Experimental set-up of DTA Instrument (built-in DTG-60H)

CHAPTER V

RESULTS AND DISCUSSION

Crystals of $NH_4^+/NiSO_4.7H_2O$ are hydrated and ionic compounds that exhibit the phase changes are found in ionic conductivity at high temperatures with dehydration. Above the transition point, electrical conductivity of the crystal enables one to classify the high temperature phases. Experimental results are presented in this chapter.

5.1 XRD Analysis

X-ray diffraction pattern was collected from powder samples of the crystal using a PC-controlled RIGAKU MULTIFLEX, automated X-ray diffractometer with monochromatic CuK_α (λ = 1.54056 Å) using Ni-filter (scan speed 4°/min). The NaI(Tl) scintillation counter was used to detect the diffracted X-rays from the sample. The measurement was taken from 10° to 70° with 2θ diffraction angle. Lattice parameters were determined from the indexed data using experimental results of low angle reflections.

Powder XRD pattern of $NH_4^+/NiSO_4.7H_2O$ crystal is shown in Fig 5.1. The observed diffraction peaks and corresponding diffraction angles (2θ), atomic spacings (d), Miller indices (hkl) and peak height of the crystal are compared with Joint Committee on Powder Diffraction Standard (JCPDS) files. Some of the experimental data are tabulated in Table 5.1. As shown in XRD pattern, the collected diffraction lines are well identified by JCPDS data files. The line at 19.50° or $(\bar{2}01)$ plane is found to the strongest in intensity among the collected XRD lines. According to XRD pattern, $NH_4^+/NiSO_4.7H_2O$ crystal belongs to orthorhombic structure at room temperature. Lattice parameters of the crystal are calculated by using the equation of $\frac{1}{d^2}=\frac{h^2}{a^2}+\frac{k^2}{b^2}+\frac{l^2}{c^2}=\frac{4\sin^2\theta}{\lambda^2}$ [19], where "d" is the atomic spacing (Å), (hkl) are miller indices, "θ" is the diffraction angle (°), "*a*", "*b*" and "*c*" are lattice parameters and "λ" is the wavelength of incident X-ray (nm).

Lattice parameters of the $NH_4^+/NiSO_4.7H_2O$ crystal are *a* = 15.69 Å, *b* = 14.24 Å and *c* = 7.06 Å respectively. Lattice parameters of the undoped Nickel Sulphate Heptahydrate, $NiSO_4.7H_2O$ crystal are *a* = 11.86 Å, *b* = 12.08 Å and *c* = 6.86 Å respectively [13, 20]. Comparison of the lattice parameters "*a*", "*b*" and "*c*" of undoped $NiSO_4.7H_2O$ and NH_4^+(1

mol%) doped $NiSO_4.7H_2O$ crystals are shown in Fig 5.2 – Fig 5.4 respectively. As shown in figures, lattice parameters "*a*", "*b*" and "*c*" of $NH_4^+/NiSO_4.7H_2O$ are found to longer than those of undoped $NiSO_4.7H_2O$. Comparison of the unit cell volume of undoped and NH_4^+(1 mol%) doped $NiSO_4.7H_2O$ crystals is shown in Fig 5.5. The volume of the unit cell of $NH_4^+/NiSO_4.7H_2O$ is larger than that of undoped $NiSO_4.7H_2O$. It is the lattice substitutions of NH_4^+ on Ni in the crystal.

5.2 FTIR Spectroscopic Analysis

FTIR transmission spectrum of NH_4^+(1 mol%) doped $NiSO_4.7H_2O$ crystal was collected on PC-controlled SHIMADZU FTIR-8400 spectrophotometer using KBr pellet method as shown in Fig 5.6. As shown in collected FTIR spectrum, wavenumbers (absorption lines) and corresponding vibrational characteristics and mode assignments of SO_4^{2-}, NH_4^+ and H_2O molecules in the crystal are tabulated in Table 5.2.

According to molecular vibrational theory, SO_4^{2-} or NH_4^+ obeys the tetrahedral pyramidal symmetry T_d-type molecule that possesses four fundamental modes of vibrations. They are ν_1-mode (A_1-species, symmetric-stretching), ν_2-mode (E-species, bending), ν_3-mode (F_2-species, dipole) and ν_4-mode (F_2-species, polarization) respectively. Normally, these four fundamental modes are Raman actives [16, 18]. Sometimes, some of the vibrational characteristics of a T_d-type molecule are Raman active but IR inactive. However, some of the vibrational characteristics of a T_d-type molecule are Raman inactive but IR active due to the mechanisms of molecular processes and optical system of spectroscopic techniques.

Furthermore, in most of the cases, SO_4^{2-} / NH_4^+ or H_2O molecules is distorted from its symmetry due to their crystalline environments. In addition, vibrational characteristics and vibrational modes may often be shifted or overlapped. Moreover, there are three types of librational motions of H_2O links molecular networks; namely, librational wagging (ν_ω), librational twisting (ν_τ) and librational rocking (ν_ρ) [16].

Ten absorption lines are observed in the FTIR spectrum. These lines are characteristics of, NH_4^+ and H_2O molecules. The lines at the wavenumbers 474 cm^{-1}, 1095 cm^{-1} / 1138 cm^{-1} and 621 cm^{-1} are represented by ν_2-mode (bending), ν_3-mode (dipole) and ν_4-modes (polarization) of SO_4^{2-}. The ν_1-mode (symmetric-stretching) of SO_4^{2-} is not found because this mode may be overlapped
under the shoulder in the wavenumber range of 800 cm^{-1} – 1000 cm^{-1} region. Normally, ν_1-mode of SO_4^{2-} is located at 980 cm^{-1}.

The line at 1434 cm^{-1} is represented by ν_4-modes (polarization) of NH_4^+. Three normal modes of NH_4^+, such as ν_1-mode (symmetric-stretching), ν_2-mode (bending) and ν_3-mode (dipole) of NH_4^+ are not found in this spectrum.

Water molecule, of course, obeys C_{2v}-symmetry and it possesses three modes of fundamental vibrations, namely; ν_1-mode (symmetric-stretching), ν_2-mode (bending), and ν_3-mode (asymmetric-stretching). Generally, their positions are shifted in liquid and solid phases. Moreover, their position may be shifted due to crystalline environments in solids. In liquid phase, e.g., pure water molecules, their positions are located at 3219 cm^{-1} (ν_1-mode), 1645 cm^{-1} (ν_2-mode) and 3405 cm^{-1} (ν_3-mode) whereas in solid phase they are normally appeared at 3200 cm^{-1}, 1640 cm^{-1} and 3400 cm^{-1} respectively [12, 16, 17]. Such shifts are taken as characteristics of solid (crystal) surrounding effects.

In the observed FTIR spectrum, two broad bands are observed with a shoulder in the wavenumber range of (1) 1600 cm^{-1} - 1900 cm^{-1} and (2) 2800 cm^{-1} - 3800 cm^{-1}. In the first range, the ν_2-mode is found at the wavenumber 1624 cm^{-1} and in the second range the ν_3-mode is appeared at 3498 cm^{-1}. The ν_1-mode of water molecule may be overlapped in the second O-H band of 2800 cm^{-1} - 3800 cm^{-1}. The absorption line at 2068 cm^{-1} is indicated by the bending vibration of CO_2.

5.3 FT-Raman Spectroscopic Analysis

FT-Raman spectrum of NH_4^+(1 mol%) doped $NiSO_4.7H_2O$ crystal was collected on PC-controlled Perkin Elmer FT-Raman spectrometer is shown in Fig 5.7. The recorded Raman lines and corresponding vibrational mode assignments of molecules in the crystal are listed in Table 5.3. Fourteen Raman lines are observed in the spectrum. The lines at 960 cm^{-1}, 468 cm^{-1}, 1003 / 1282 cm^{-1} and 647 cm^{-1} are represented by the four normal modes of SO_4^{2-}. They are ν_1-mode, ν_2-mode, ν_3-mode and ν_4-mode respectively.

The Raman lines at 3158 cm^{-1} and 1459 cm^{-1} are represented by two normal modes of NH_4^+. It is indicated by the NH_4^+ dopant effect of $NiSO_4.7H_2O$ crystal. The lines at 3273 cm^{-1}, 1625 cm^{-1} and 3573 cm^{-1} are represented by three normal modes of H_2O molecules. They are ν_1-mode, ν_2-mode and ν_3-mode respectively.

Librational twisting and librational rocking vibrations of (SO_4---H_2O---SO_4) molecular networks are found at 787 cm^{-1} and 855 cm^{-1} respectively. Moreover, the Raman lines at 2598 cm^{-1} and 2711 cm^{-1} are represented by the stretching vibrations of (O---S---O) in SO_4. The Raman line at 2598 cm^{-1} is the strongest in intensity among the observed Raman lines because the intensity of stretching vibration of molecule is more intense than bending vibration in a Raman spectrum.

5.4 Temperature Dependent Electrical Conductivity and Dielectric Analyses

Electrical conductivity of an ionic material obeys an Arrhenius expression $\sigma = \sigma_0 \exp(-E_i / kT)$, where σ is the conductivity, or ion drift in materials, σ_0 is the pre-exponential factor or slope of the conductivity curve, $E_i = E_j + \Delta H_s / 2$, E_i is the activation energy for ionic conduction, E_j is the barrier height, ΔH_s is thermal changes of Schottky defects accompanying the cation vacancy plus anion vacancy and ion vacancy plus interstitial ion, *k* is the Boltzmann constant and T is the absolute temperature [2, 14]. Arrhenius plot of the variation of dc electrical conductivity of the NH_4^+(1 mol%) doped $NiSO_4.7H_2O$ crystal in the temperature range of 300 K to 543 K is shown in Fig 5.8. According to the theory of ionic conductivity, the slope of the electrical conductivity in Fig 5.8 corresponding to the activation energy for creating of defect states due to the dehydration of water of the crystal. The electrical conductivity (σ) of the crystal for $T \geq T_{dehydration}$ can be written in the form:

$$\sigma = \sigma_0 \exp(-E_i / kT)$$
$$\ln\sigma = -E_i / kT + \ln\sigma_0$$
$$= (-E_i / k)(1/T) + \ln\sigma_0$$

Comparing the above equation with the experimental linear equation, $y = mx + c$, where the value of slope will give the value of ($-E_i/k$). From Fig 5.9, the activation energy E_i can be obtained by using the slope of the ln(σ) versus 10^3/T graph. From Fig 5.9, the activation energy and electrical conductivity of the crystal are calculated as 0.97 eV and 7.73 x 10^{-9} S cm^{-1} at the temperature of 397 K, and it is the dehydration temperature ($T_{dehydration}$) of the crystal from $NH_4^+/NiSO_4.7H_2O$ to $NH_4^+/NiSO_4.H_2O$ (heptahydrate to monohydrate).

However, the activation energy of the sample under the dehydration temperature ($T < T_{dehydration}$) is about 0.39 eV and temperature dependent electrical conductivity curve under the dehydration temperature of the sample is shown in Fig 5.10. From the temperature dependent electrical conductivity results, the calculated activation

energy and electrical conductivity of the crystal over the decomposition temperature ($T \geq T_{dehydration}$) are greater than that of before the dehydration temperature. It shows the normal ionic conductivity ($<10^{-5}$ S cm^{-1}) of the sample. Thus, crystal of NH_4^+(1 mol%) doped $NiSO_4.7H_2O$ is a normal ionic conductor at high temperature.

Plot of the resistivity (ρ) and conductivity (σ) versus temperature of the crystal are shown in Fig 5.11 in which the intersection of two curves (ρ & σ) at about 397 K can be taken as the dehydration temperature. As shown in figure, electrical conductivities of the crystal are increased with increasing temperatures and electrical resistivities, however, are decreased with increasing temperatures. From the plot, the intersection of resistivity (ρ) and conductivity (σ) curves shows the dehydration temperature ($T_{dehydration}$) of the crystal.

Temperature dependent dielectric constants of the crystal are shown in Fig 5.12. It is found that dielectric constants of the crystal are generally increased with increasing temperatures. Experimental results of temperature dependent electrical conductivity and dielectric constants are tabulated in Table 5.4.

5.5 TG-DTA Analysis

The TG and DTA thermograms of NH_4^+(1 mol%) doped $NiSO_4.7H_2O$ crystal are shown in Fig 5.13. The percentage weight losses observed in TG, tally with the following formulated decomposition pattern.

$$NH_4^+ / NiSO_4.7H_2O \xrightarrow{(63°\text{-}576\ °C)} NH_4^+ / NiSO_4.H_2O + 6H_2O$$

In this step, NH_4^+ / $NiSO_4.7H_2O$ crystal undergoes to NH_4^+ / $NiSO_4.H_2O$ crystal with the removal of six water ($6H_2O$) molecules on heating between 63°C and 576°C with the weight loss is about 43.94 % with dehydration process. After the temperature at about 350°C, the crystal melted due to the continuous heating.

The strong endothermic reaction peak in DTA curve found at 124°C that indicates the removal of six water molecules or dehydration of six water molecules from the $NH_4^+/NiSO_4.7H_2O$ (heptahydrate) material to $NH_4^+/NiSO_4.H_2O$ crystal (monohydrate).

5.6 Conclusion

Crystals of NH_4^+(1 mol%) doped $NiSO_4.7H_2O$ were grown by the slow evaporation of aqueous solution. Structure, vibrational and thermal characteristics of the crystal were studied by XRD, FTIR, FT-Raman, temperature dependent electrical conductivities and TG-DTA methods.

- According to XRD pattern, NH_4^+(1 mol%) doped $NiSO_4.7H_2O$ crystal belongs to orthorhombic structure. Lattice parameters of the crystal are a = 15.69 Å, b = 14.24 Å and c = 7.06 Å respectively.

- From the observed FTIR spectrum, ten absorption lines are found in the spectrum. These lines are vibrational characteristics of five different molecules. From the observed FT-Raman spectrum, fourteen Raman lines are found and these lines are vibrational characteristics of five different molecules.

- Temperature dependent electrical conductivities and dielectric constants of the crystal are increased with increasing temperatures. The activation energies, electrical conductivities and dielectric constants of the crystal are studied in detailed. From the temperature dependent electrical conductivities and dielectric measurements, dehydration temperature ($T_{dehydration}$) of the crystal is 397 K in which the crystal of $NH_4^+/NiSO_4.7H_2O$ undergoes $NH_4^+/NiSO_4.H_2O$.

- Dehydration temperature ($T_{dehydration}$) of the crystal is well conformed by TG-DTA method. According to experimental results, $NH_4^+/NiSO_4.7H_2O$ crystal can be considered as the oscillator and solid electrolyte materials.

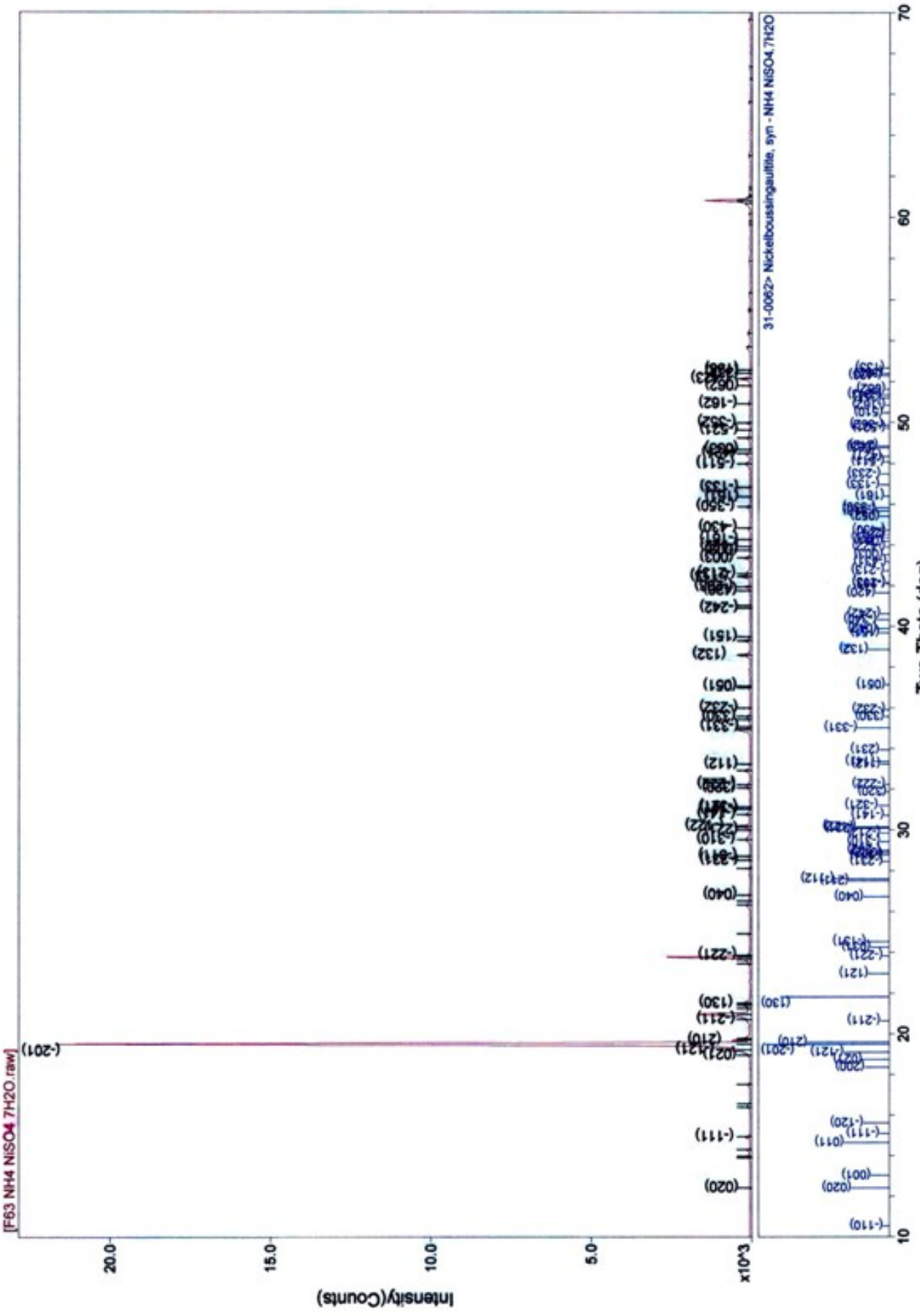

Fig 5.1 XRD pattern of NH_4(1 mol%) doped $NiSO_4.7H_2O$ crystal

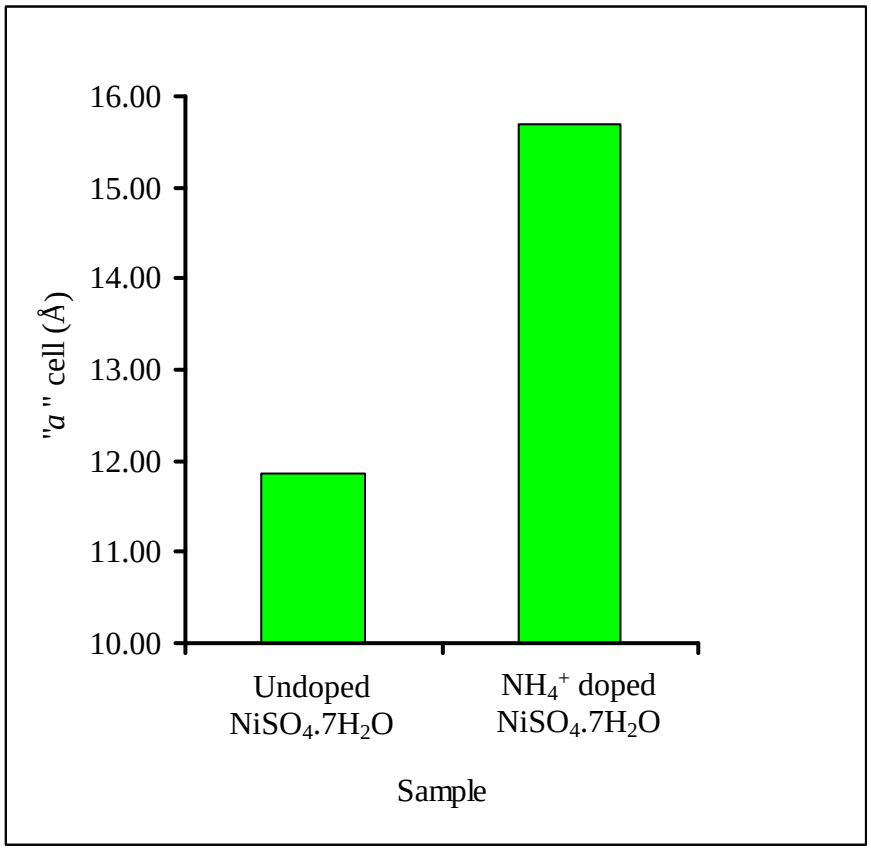

Fig 5.2 Comparison of the length of lattice parameter "*a*" of undoped $NiSO_4.7H_2O$ and NH_4^+(1 mol%) doped $NiSO_4.7H_2O$ crystals

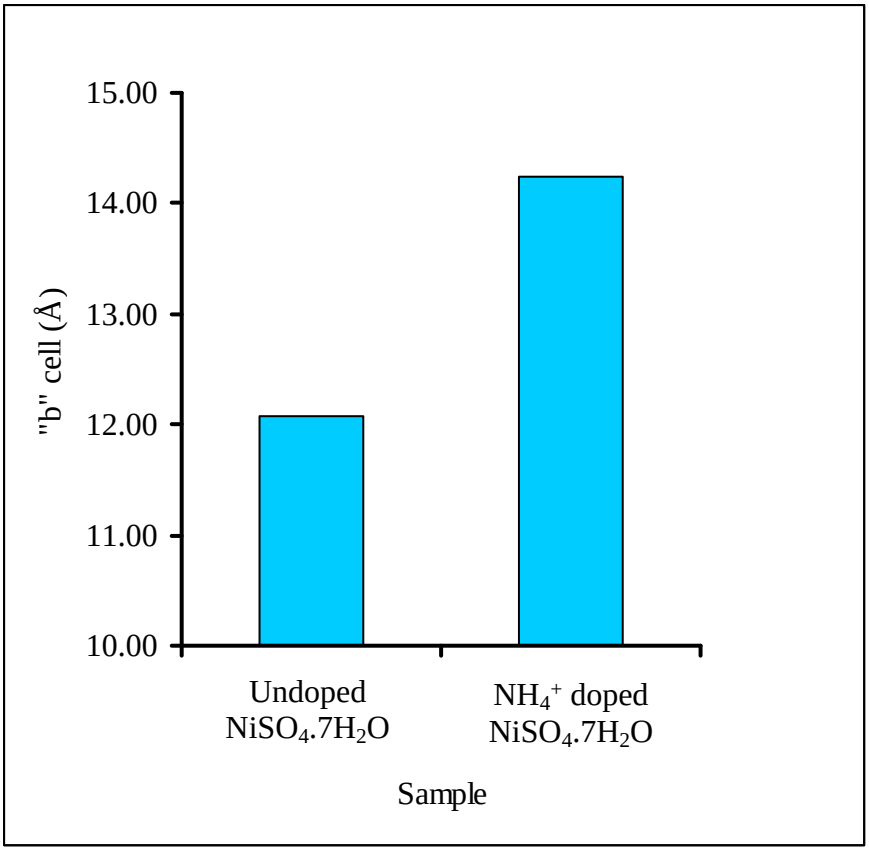

Fig 5.3 Comparison of the length of lattice parameter "*b*" of undoped $NiSO_4.7H_2O$ and NH_4^+(1 mol%) doped $NiSO_4.7H_2O$ crystals

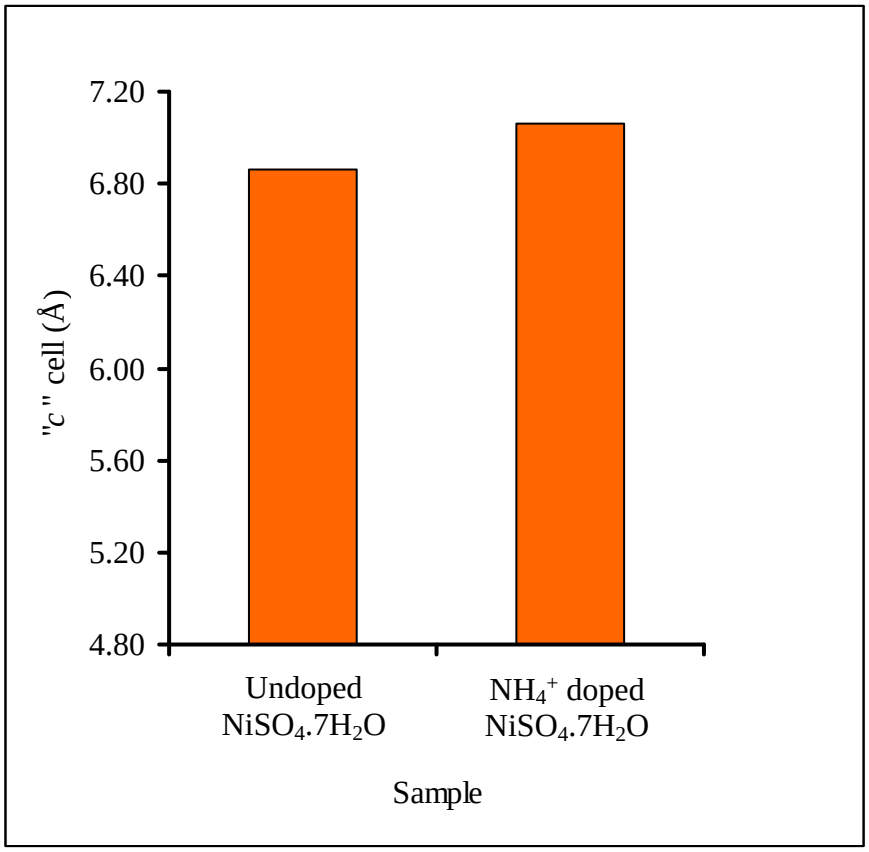

Fig 5.4 Comparison of the length of lattice parameter "*c*" of undoped $NiSO_4.7H_2O$ and NH_4^+(1 mol%) doped $NiSO_4.7H_2O$ crystals

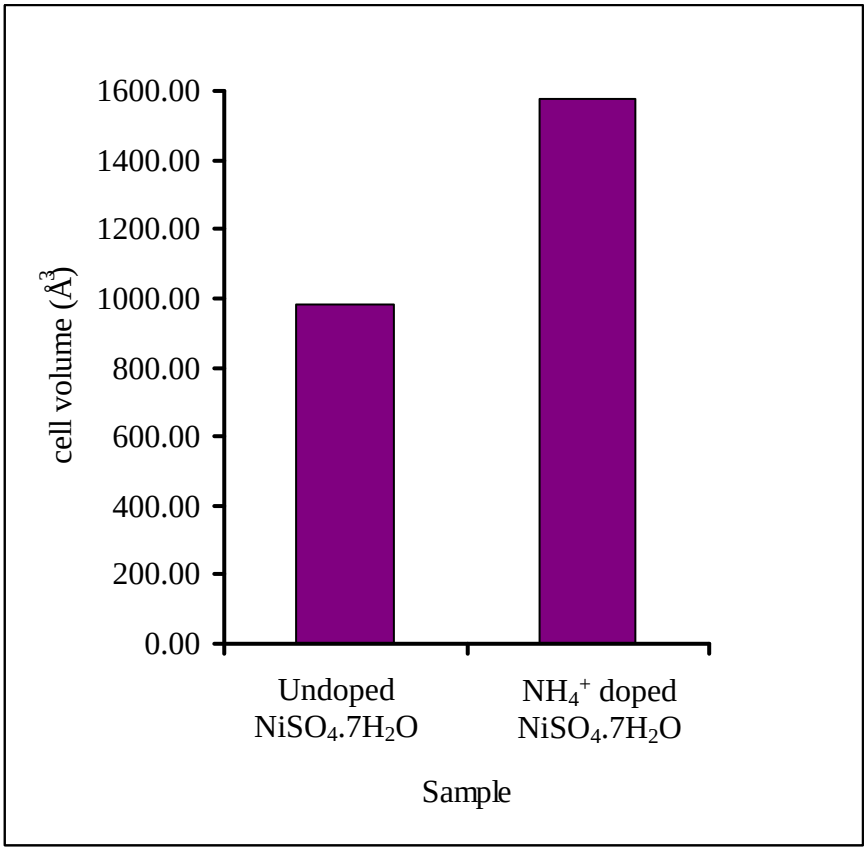

Fig 5.5 Comparison of unit cell volume of undoped $NiSO_4.7H_2O$ and NH_4^+(1 mol%) doped $NiSO_4.7H_2O$ crystals

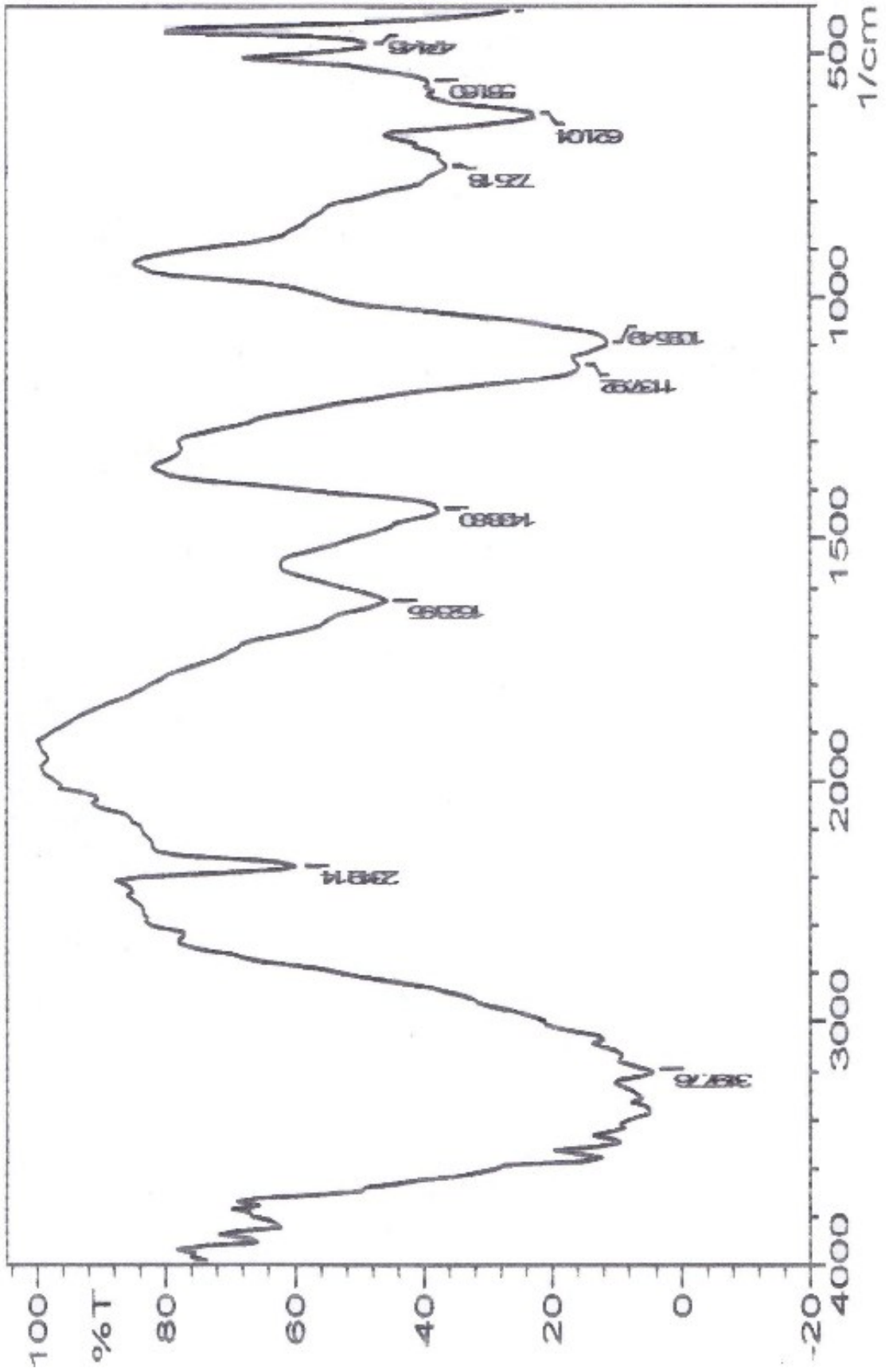

Fig 5.6 FTIR transmission spectrum of NH_4^+(1 mol5) doped $NiSO_4.7H_2O$ crystal

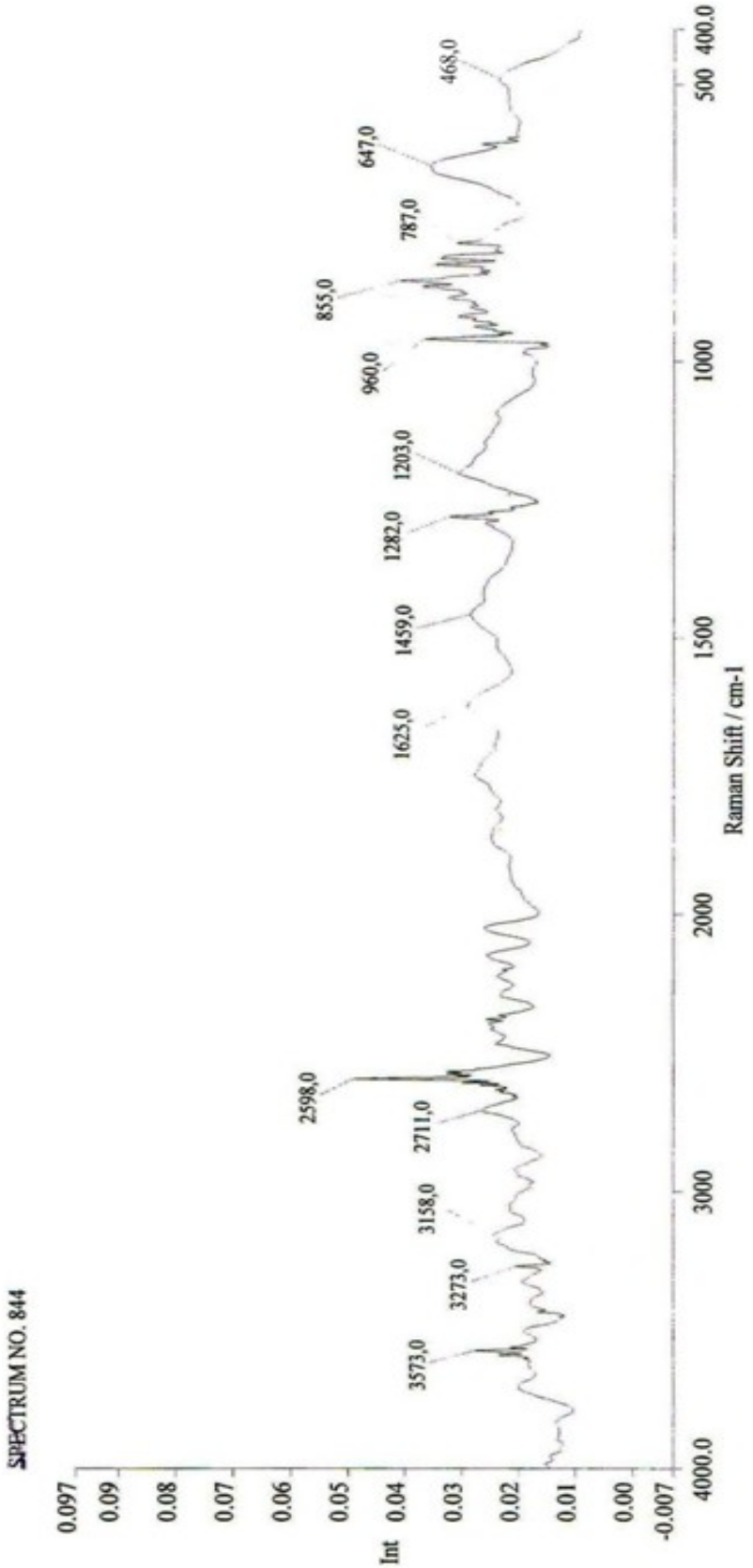

Fig 5.7 FT-Raman spectrum of NH_4^+(1 mol%) doped $NiSO_4.7H_2O$ crystal

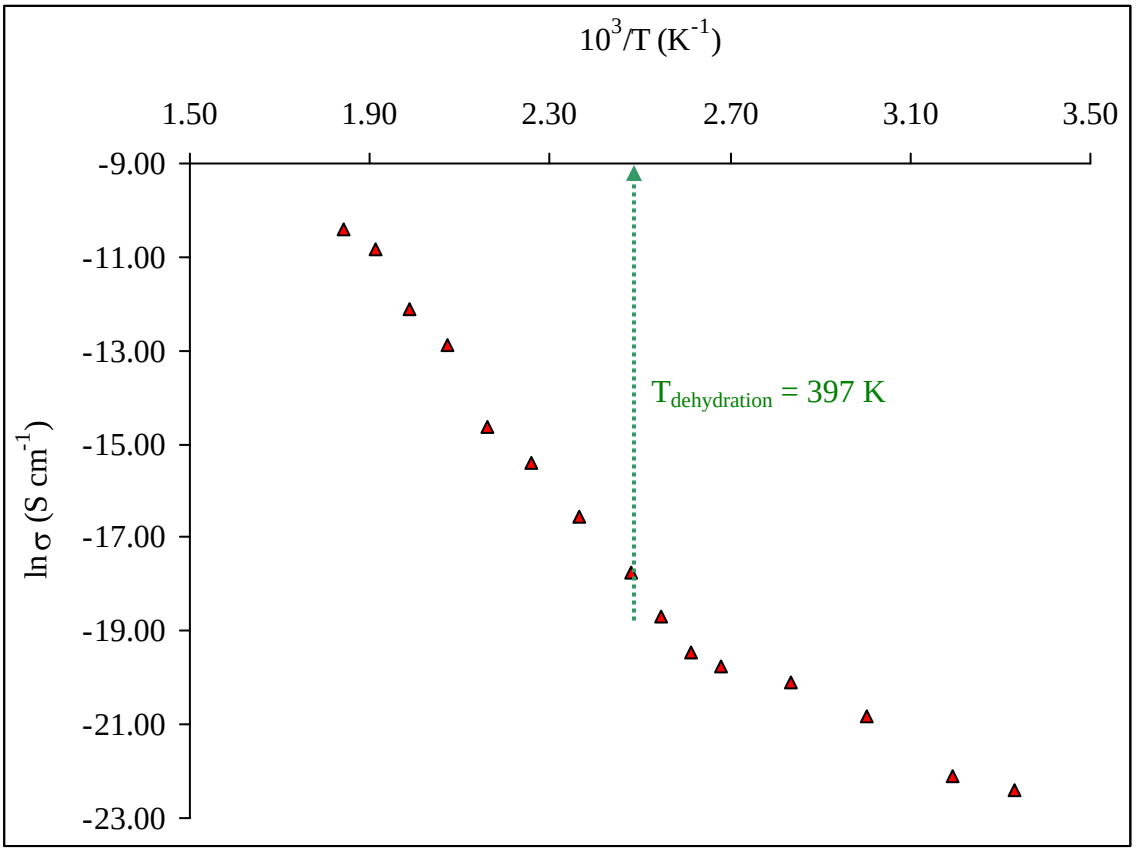

Fig 5.8 Arrhenius plot of the temperature dependent electrical conductivity of NH_4^+(1 mol%) doped $NiSO_4.7H_2O$ crystal

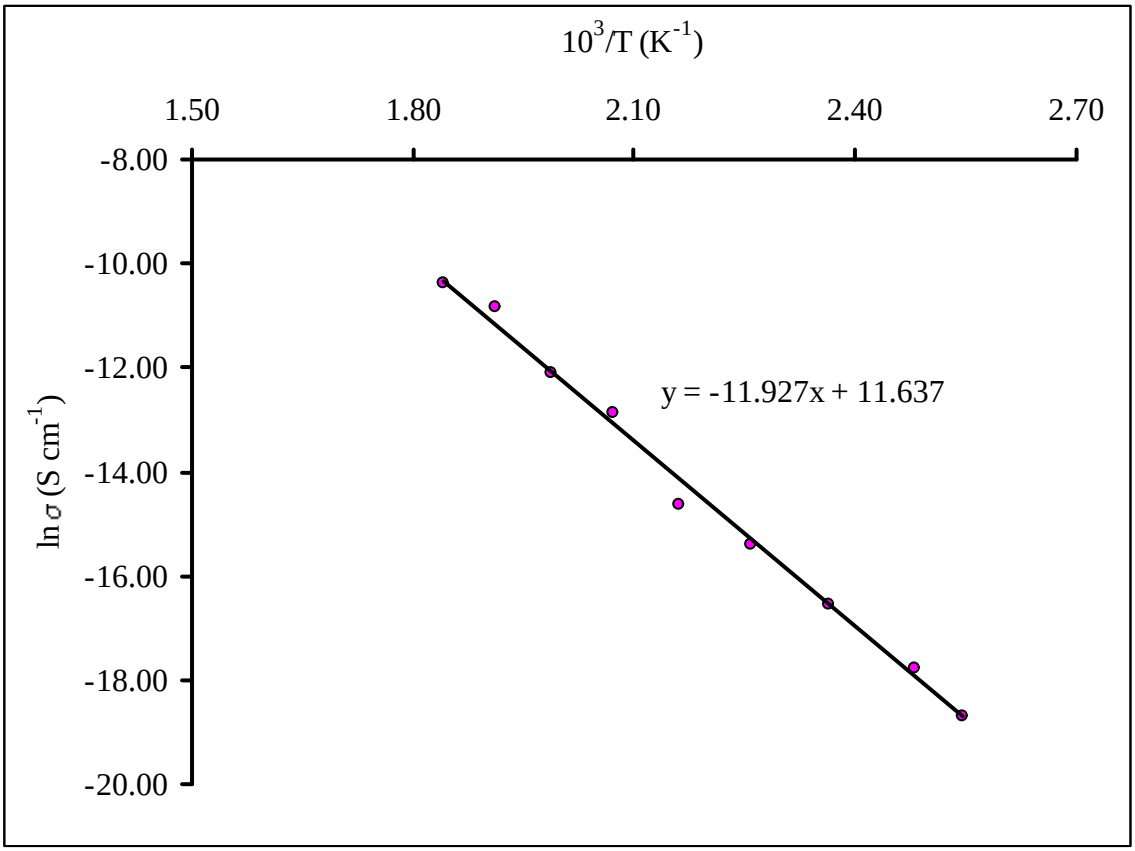

Fig 5.9 Temperature dependent electrical conductivity of NH_4^+(1 mol%) doped $NiSO_4.7H_2O$ crystal for temperature $T \geq T_{dehydration}$ (397 K)

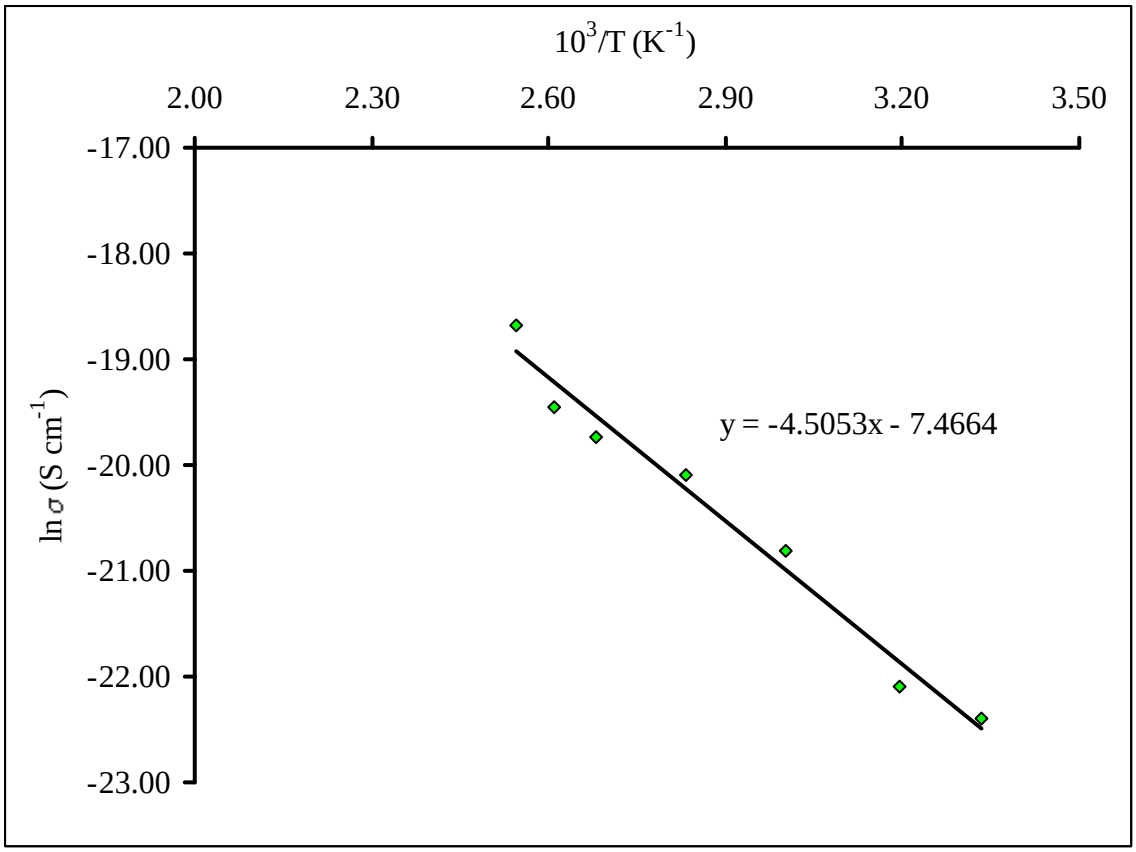

Fig 5.10 Temperature dependent electrical conductivity of NH_4^+(1 mol%) doped $NiSO_4.7H_2O$ crystal for temperature $T<T_{dehydration}$ (397 K)

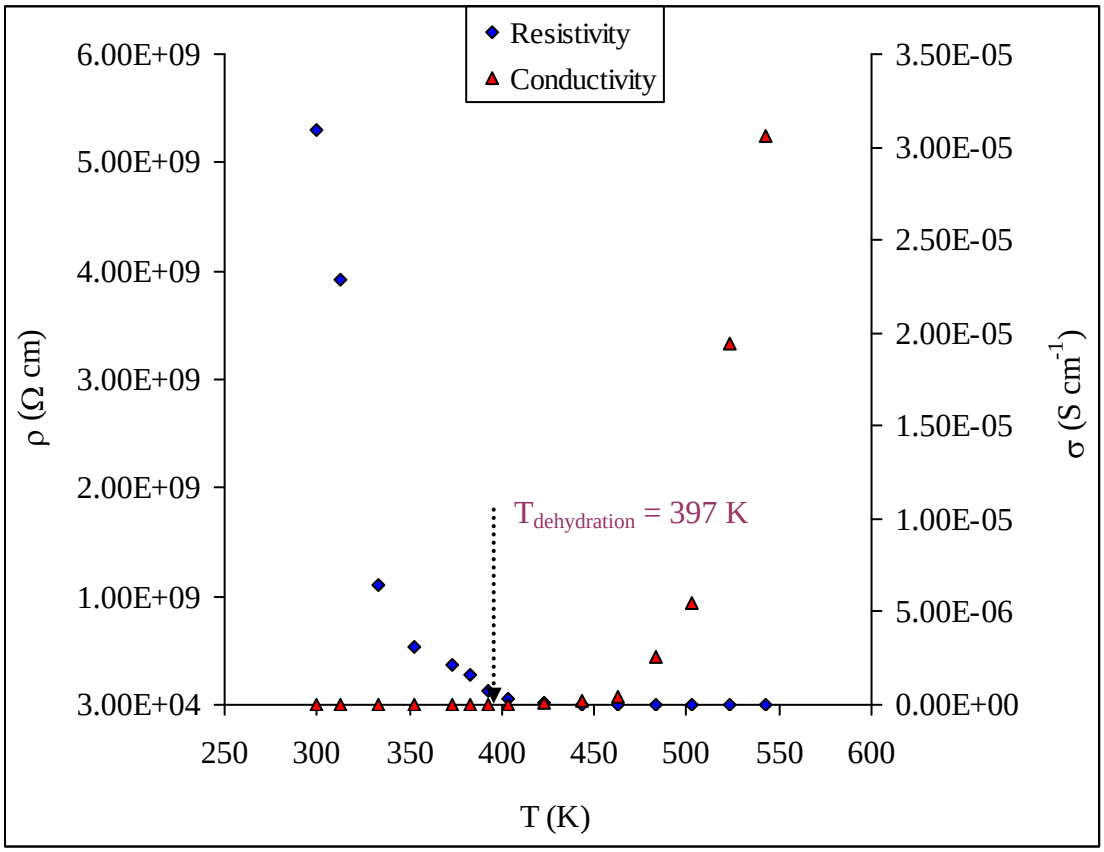

Fig 5.11 Plot of the variation of the resistivity (ρ) and conductivity (σ) with temperature (T) of $NH_4^+/NiSO_4.7H_2O$ crystal

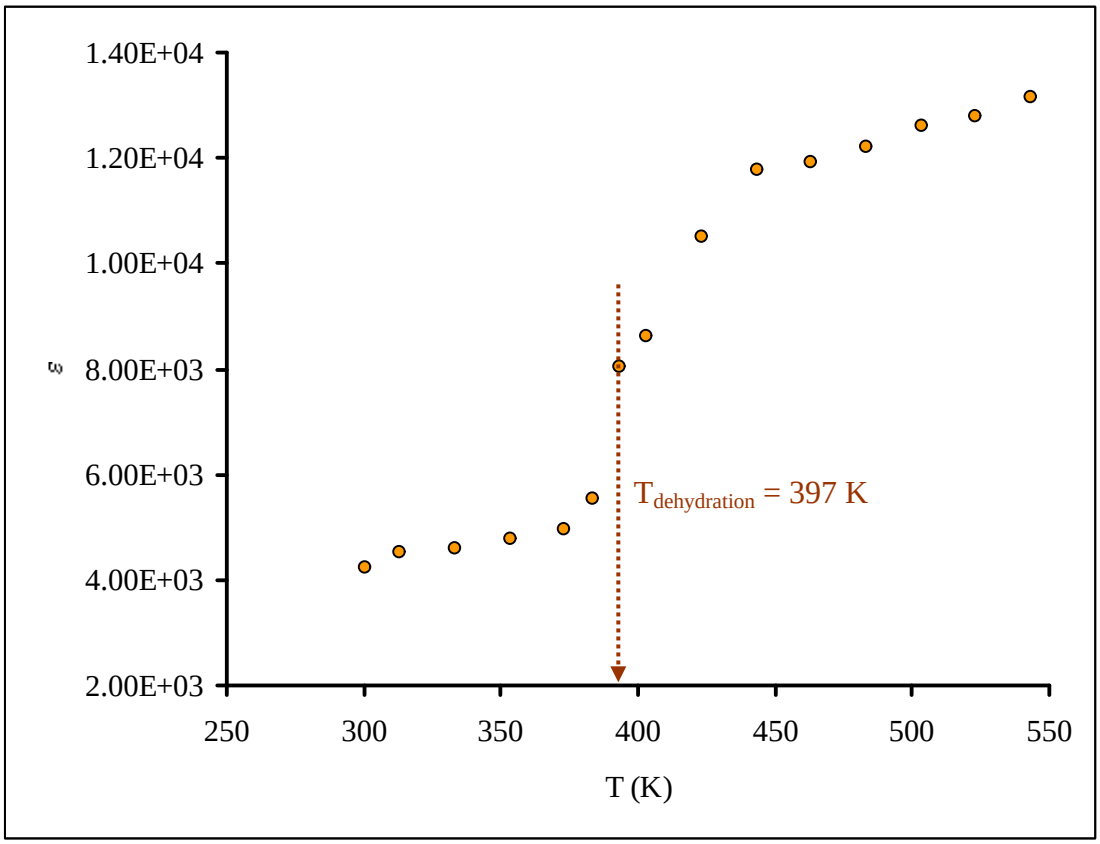

Fig 5.12 Temperature dependent dielectric constants of NH_4^+(1 mol%) doped $NiSO_4.7H_2O$ crystal

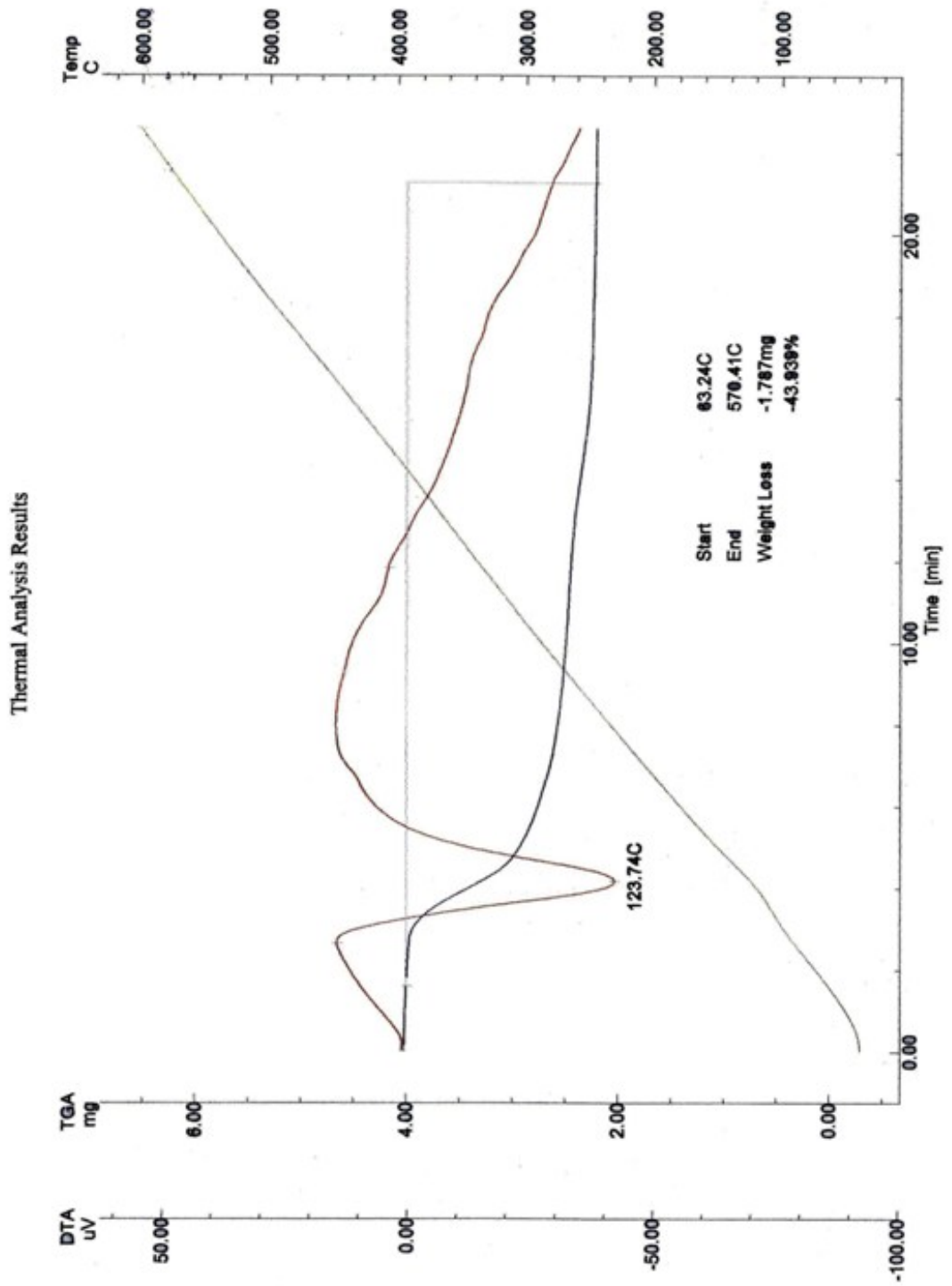

Fig 5.13 TG-DTA thermograms of NH_4^+(1 mol%) doped $NiSO_4.7H_2O$ crystal

Table 5.1 XRD data of NH_4^+(1 mol%) doped $NiSO_4.7H_2O$ crystal

Line No	2θ (°)	*d* (Å)	(hkl)	I (%)
1	12.42	7.12	(020)	0.10
2	14.94	5.93	$(\bar{1}11)$	0.80
3	18.96	4.68	(021)	0.30
4	19.22	4.61	$(\bar{1}21)$	3.50
5	19.50	4.55	$(\bar{2}01)$	100.00
6	19.69	4.50	(210)	2.50
7	20.72	4.28	$(\bar{2}11)$	0.50

Table 5.2 Wavenumbers and corresponding vibrational mode assignments of NH_4^+(1 mol%) doped $NiSO_4.7H_2O$ crystal

Line No	Wavenumbers (cm^{-1})	Mode Assignments	Vibrational characteristics
1	474	$\nu_2(SO_4^{2-})$	Bending
2	552	$\nu_\omega(Ni\text{---}H_2O\text{---}NH_4)$	Librational wagging
3	621	$\nu_4(SO_4^{2-})$	Polarization
4	725	$\nu_\tau(SO_4\text{---}\ H_2O\text{---}SO_4)$	Librational twisting
5	1095/1138	$\nu_3(SO_4^{2-})$-splitting	Dipole
6	1434	$\nu_4(NH_4^+)$	Polarization
7	1624	$\nu_2(H_2O)$	Bending
8	2349	$\nu(CO_2)$	Bending (due to KBr)
9	3498	$\nu_3(H_2O)$	Asymmetric-stretching

Table 5.3 Raman shifts and corresponding vibrational mode assignments of Li^{3+}(1 mol%) doped $NiSO_4.7H_2O$ crystal

Line No	Raman shift (cm^{-1})	Mode Assignments	Vibrational characteristics
1	468	$\nu_2(SO_4^{2-})$	Bending
2	647	$\nu_4(SO_4^{2-})$	Polarization
3	787	$\nu_\tau(SO_4\text{---}H_2O\text{---}SO_4)$	Librational twisting
4	855	$\nu_\rho(SO_4\text{---}\ H_2O\text{---}SO_4)$	Librational rocking
5	960	$\nu_1(SO_4^{2-})$	Symmetric-stretching
6	1203 / 1282	$\nu_3(SO_4^{2-})$-splitting	Dipole
7	1459	$\nu_4(NH_4^+)$	Polarization
8	1625	$\nu_2(H_2O)$	Bending
9	2598, 2711	ν(O---S---O)	Stretching
10	3158	$\nu_3(NH_4^+)$	Dipole
11	3273	$\nu_1(H_2O)$	Symmetric-stretching
12	3573	$\nu_3(H_2O)$	Asymmetric-stretching

Table 5.4 Experimental results of temperature dependent electrical conductivity and dielectric constants of NH_4^+(1 mol%) doped $NiSO_4.7H_2O$ crystal

T (°C)	$10^3/T$ (K^{-1})	R (Ω)	ρ (Ω cm)	σ (S cm^{-1})	ε
27	3.33	9.10E+08	5.31E+09	1.88E-10	4.24E+03
40	3.19	6.73E+08	3.92E+09	2.55E-10	4.54E+03
60	3.00	1.89E+08	1.10E+09	9.10E-10	4.62E+03
80	2.83	9.20E+07	5.36E+08	1.86E-09	4.79E+03
100	2.68	6.42E+07	3.74E+08	2.67E-09	4.99E+03
110	2.61	4.82E+07	2.81E+08	3.56E-09	5.55E+03
120	2.54	2.22E+07	1.29E+08	7.73E-09	8.07E+03
130	2.48	8.85E+06	5.16E+07	1.94E-08	8.62E+03
150	2.36	2.60E+06	1.52E+07	6.60E-08	1.05E+04
170	2.26	8.50E+05	4.96E+06	2.02E-07	1.18E+04
190	2.16	3.94E+05	2.30E+06	4.35E-07	1.19E+04
210	2.07	6.68E+04	3.89E+05	2.57E-06	1.22E+04
230	1.99	3.12E+04	1.82E+05	5.51E-06	1.26E+04
250	1.91	8.82E+03	5.14E+04	1.94E-05	1.28E+04
270	1.84	5.60E+03	3.27E+04	3.06E-05	1.32E+04

$l/A = 14.8\ cm^{-1}$

REFERENCES

1. Bolton W 1991 "Instrumentation & Measurement" (Oxford: Newnes)
2. Callister W D 2001 “Fundamentals of Materials Science and Engineering” (New York: Wiley)
3. Chung D D L 2001 “Applied Materials Science” (Boca Raton: CRC)
4. Clegg W 2003 "Crystal Structure Determination" (Oxford: Oxford Science)
5. Freeda T H & Mahadevan C 2001 PRAMANA-Journal of Physics 57 (4) 829
6. Gaulitz G & Vo-Dinh T 2003 “Handbook of Spectroscopy” (New York: Wiley) 7. Hollas J M 2004 “Modern Spectroscopy” (New York: Wiley)
8. Kanagadurai R et al 2009 E-Journal of Chemistry 6 (3) 871
9. Karan S & Gupta S 2005 Materials Science and Engineering 395 198
10. Kasatkin I A 2002 Crystal Research Technology 37 (2-3) 193
11. Kittle C 1999 "Introduction to Solid State Physics" (Singapore: Wiley)
12. Kumari M S & Secco E A 1983 Canadian Journal of Chemistry 61 599
13. Long D A 1988 "Raman Spectroscopy" (New York: Wiley)
14. Pillai S O 2006 "Solid State Physics" (New Delhi: New Age)
15. Raj C J et al 2007 Crystal Research Technology 42 (4) 344
16. Ross S D 1972 "Inorganic Infrared and Raman Spectra" (London: McGraw-Hill)
17. Shackelford J F & Alexander W 2001 “Materials Science and Engineering Handbook” (Boca Raton: CRC)
18. Singh K et al 1995 Bulletins Materials Science 18 (2) 147
19. Stuart B & Ando D J 1996 "Modern Infrared Spectroscopy" (New York: Wiley)
20. Suryanarayana C & Norton M G 1998 "X-Ray Diffraction A Practical Approach" (New York: Plenum)
21. Theivanayagom M & Mahadevan C 2001 Bulletins Material Science 24 (5) 441
22. Yadav M S 2003 “A Textbook of Spectroscopy” (New Delhi: Anmol)
23. 2001 "Handout on Basic Principles of DTG-60/60H" (Kyoto: Shimadzu)
24. 2008 Encyclopedia Britannica Library (Oxford: Oxford University)